

Modular pincer-type pyridylidene amide (PYA) ruthenium(II) complexes for efficient transfer hydrogenation catalysis

Philipp Melle, Yanisha Manoharan and Martin Albrecht*

Department für Chemie und Biochemie, Universität Bern, Freiestrasse 3, CH-3012 Bern, Switzerland.

email: martin.albrecht@dcb.unibe.ch

Abstract

A set of bench-stable ruthenium complexes with new *N,N,N*-tridentate coordinating pincer-type pyridyl-bis(pyridylideneamide) ligands was synthesized in excellent yields, with the pyridylidene amide in *meta* or in *para* position (*m*-PYA and *p*-PYA, respectively). While complex $[\text{Ru}(\textit{p}\text{-PYA})(\text{MeCN})_3]^{2+}$ is catalytically silent in transfer hydrogenation, its *meta* isomer $[\text{Ru}(\textit{m}\text{-PYA})(\text{MeCN})_3]^{2+}$ shows considerable activity with turnover frequencies at 50% conversion $\text{TOF}_{50} = 100 \text{ h}^{-1}$. Spectroscopic, electrochemical, and crystallographic analyses suggest considerably stronger donor properties of the zwitterionic *m*-PYA ligand compared to the partially π -acidic *p*-PYA analogue, imparted by valence isomerization. Further catalyst optimization was achieved by exchanging the ancillary MeCN ligands with imines (4-picoline), amines (ethylenediamine), and phosphines (PPh_3 , dppm, dppe). The most active catalyst was comprised of the *m*-PYA pincer ligand and PPh_3 , complex $[\text{Ru}(\textit{m}\text{-PYA})(\text{PPh}_3)(\text{MeCN})_2]^{2+}$, which reached a TOF_{50} of 430 h^{-1} under aerobic conditions and up to $4,000 \text{ h}^{-1}$ in the absence of oxygen. The presence of oxygen reversibly deactivates the catalytically active species, which compromises activity, but not longevity of the catalyst. Ligand exchange kinetic studies by NMR spectroscopy indicate that the strong *trans* effect of the phosphine is critical for high catalyst activity. Diaryl, aryl-alkyl, and dialkyl ketones were hydrogenated with high conversion, and α,β -unsaturated ketones produced selectively the saturated ketone as the only product due to exclusive C=C bond hydrogenation, a distinctly different selectivity from most other transfer hydrogenation catalysts.

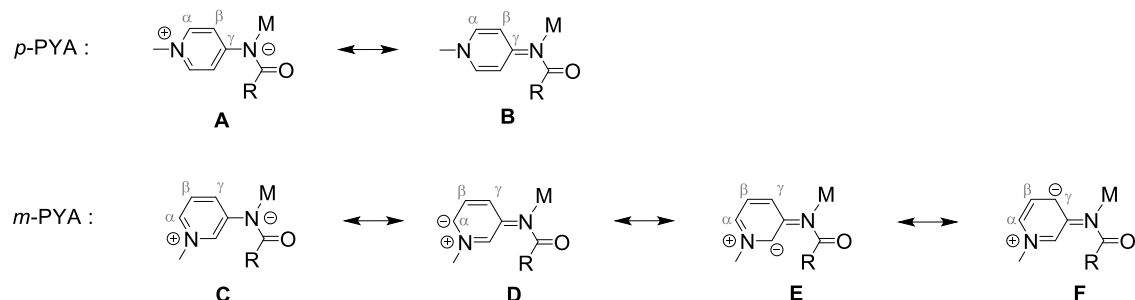
Introduction

The pincer ligand motif is typically comprised of a meridional tridentate donor system and has attracted considerable interest as a platform for organometallic and inorganic chemistry.^{1–10} Originally, the pincer platform has been confined to an ECE donor system with a central carbanion and flanking phosphines (E = P)¹¹ or amines (E = N).^{12,13} Complexes with this ECE pincer motif feature a remarkably robust C–M bond, which enabled the stabilization of a variety of otherwise highly reactive transition states, *e.g.* for transmetalation,^{14,15} oxidative addition,¹⁶ or C–C bond making and breaking reactions.^{17–21} The pincer platform has been continuously expanded to include a variety of donor combinations.² A particularly versatile and catalytically competent variation includes pincer ligands containing a central pyridyl unit such as PNP and PNN pincer ligands, often referred to as the Milstein system.^{22–25} In these ligands, the central aromatic ring features a lower resonance stabilization energy compared to the benzene ring in aryl-based ECE pincer ligands, which favors deprotonation of the benzylic position and formation of an exocyclic double bond with concomitant pyridine dearomatization. Since this process is reversible, these pincer ligands provide a scaffold for reversible proton storage and release.^{24,26} These ligands are therefore non-innocent and when coordinated to a suitable metal, the complexes offer bifunctionality for efficient catalysis,^{27–30} similar to Noyori's or Shvo's catalyst.^{31,32} This non-innocence of the pincer ligand has been explored by using variations on the theme, including aliphatic backbones³³ as well as different central heterocycles.³⁴

In all these pincer ligands, (de)protonation reversibly changes the ligand donor properties from a neutral imine to a formally anionic amide. We have been intrigued by the possibility to install similar donor flexibility by using resonance flexibility, which does not require the transfer of a proton. Pyridylidene amides (PYAs)^{35–43} offer excellent prospects for such applications, as they exist in two limiting resonance forms: a zwitterionic form with an amide coordination site (**A**, Scheme 1) and a neutral imine form (**B**, Scheme 1). Accordingly, the donor properties of this ligand can be modulated by external factors such as the coordinated metal and its spectator ligands and by the polarity of the solvent.^{44–46} The flexibility imparts catalytic activity, and is further modulated upon alteration of the pyridine substitution pattern from *para*-PYAs (**A**, **B**) to *meta*-PYA scaffolds (**C**, Scheme 1).⁴⁷ Of note, such *meta*-PYA ligands cannot be represented by a neutral resonance structure and feature only zwitterionic structures.⁴⁸ Provided resonance structures **D–F** are also relevant, then these ligands are mesoionic *N*-donor systems,⁴⁹ related to mesoionic *N*-heterocyclic carbenes.^{50–52}

The ligand flexibility imparted by these PYA systems offers intriguing opportunities for the stabilization of different metal electronic configurations without the need of chemical transformation of the ligand skeleton. Therefore, we were particularly intrigued by combining the very successful pincer motif and the PYA donor systems to develop catalysts for redox transformations. Here we now present a new member of the pincer family comprised of PYA donors. We demonstrate the electronic control that is exerted by the PYA donors

on the coordinated ruthenium center, as well as catalytic application in transfer hydrogenation. The catalytic activity is optimized by the choice of PYA system as well as the spectator ligands, which allowed turnover numbers to be continuously raised from 100 to 4,000 h⁻¹.

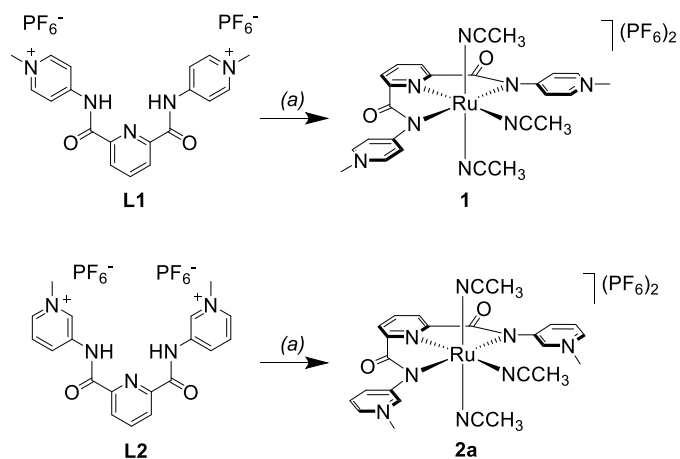


Scheme 1. Limiting resonance structures of *para*-PYA (top) and *meta*-PYA ligands.

Results and Discussion

Synthesis of generic bis-PYA pincer ruthenium complexes. The two PYA pincer ligand precursors **L1** and **L2** (Scheme 2) were obtained from the corresponding iodide salts, which were prepared in two straightforward steps according to literature procedures⁵³. Anion exchange was performed to avoid iodide ions in the metal complexes, as iodides tend to interfere with redox transformations and was achieved by heating the iodide salts with an excess of NH₄PF₆ in a H₂O/MeCN mixture (Fig. S1).

The dicationic pincer ruthenium(II) complexes **1** and **2a** with *para* and *meta*-PYA pincer arms, respectively, were synthesized in excellent yields (>90%) by an *in situ* deprotonation/metalation procedure using Na₂CO₃ and [RuCl₂(cym)]₂ (Scheme 1). This procedure avoids the formation of the neutral free ligand. Complexation was indicated macroscopically by a color change of the reaction mixture from orange to deep red. Complexes **1** and **2a** are air- and moisture stable and have been purified by repetitive precipitation.



Scheme 2. Synthesis of Ru(II) PYA pincer complexes **1** and **2a**. Reactions and conditions: (a) 0.5 eq. $[\text{RuCl}_2(\text{cym})]_2$; 3 eq. Na_2CO_3 in MeCN, reflux, 16 h.

Evidence for the formation of the complexes was obtained by ^1H NMR spectroscopy, which showed the loss of the amide proton resonances at $\delta_{\text{H}} = 11.95$ and 11.67 from **L1** and **L2**, respectively. Moreover, the pyridyl proton resonances of the PYA unit shifted markedly upfield upon ruthenation. For example, the two doublets appearing at $\delta_{\text{H}} = 8.87$ and 8.49 in **L1** resonate at about 0.5 ppm higher field in the ruthenium complex **1** ($\delta_{\text{H}} = 8.52$ and 7.91). Similar shift differences were observed for complex **2a** in comparison to the resonances of **L2**. The resonances of the coordinated MeCN ligands appear as two distinct singlets in 2:1 integral ratio around $\delta_{\text{H}} = 2.3$ and 2.7 for the two axial and the in-plane ligands, respectively, suggesting no significant ligand exchange in $\text{DMSO}-d_6$. The resonances of the axial MeCN ligands are identical in both complexes, while the equatorial ligand is less shielded in **1** ($\delta_{\text{H}} = 2.76$) than in **2a** ($\delta_{\text{H}} = 2.65$), indicative of a stronger donation of the *m*-PYA ligand compared to the *para* isomer. High resolution MS of the complexes showed the characteristic isotopic signature of ruthenium together with the expected m/z signal at 676.0590 (676.0593 calculated for $[\mathbf{1}-\text{MeCN}-\text{PF}_6]^+$) and $m/z = 717.0859$ (717.0862 calculated for $[\mathbf{2}-\text{PF}_6]^+$; Fig. S2, S3).

Crystal structure analysis. Single crystal X-ray diffraction analysis of complexes **1** and **2a** confirmed the structural assignment (Fig. 1). The molecular structures of complexes **1** and **2a** both feature a ruthenium center in distorted octahedral geometry with a *N,N,N*-tridentate *mer*-chelating bis-PYA pincer ligand and three MeCN spectator ligands. The most severe distortion is entailed by the relatively small bite angle of the bis-PYA pincer ligand, which is identical within esds for complexes **1** and **2a** ($157.82(14)^\circ$ and $157.55(8)^\circ$, respectively) and considerably smaller than the ideal 180° .

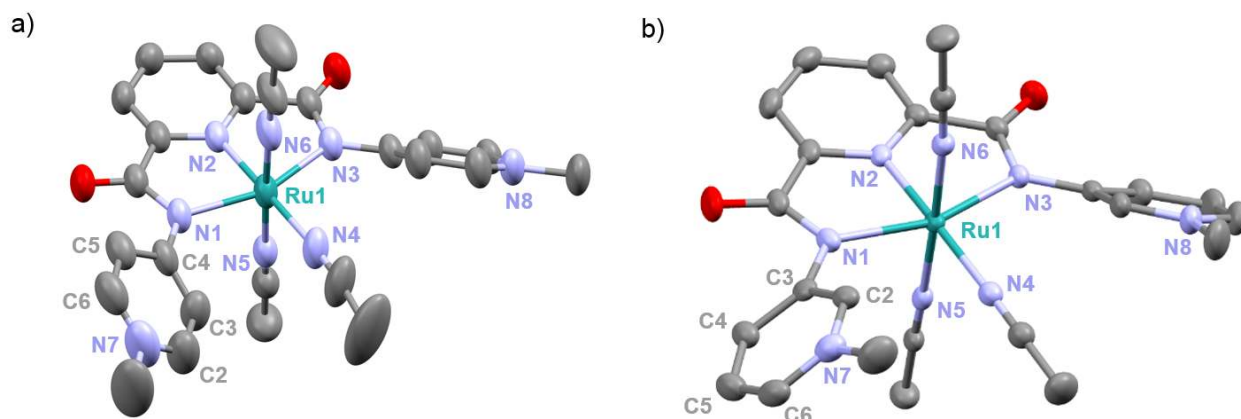


Figure 1. ORTEP representations of the complex cations **1** (a) and **2a** (b); all ellipsoids at 50% probability level (hydrogen atoms, non-coordinating PF_6^- anions, co-crystallized solvent molecules, and conformational disorder of the methyl-pyridinium groups omitted for clarity).

The metrics around the ruthenium center are almost identical for both complexes. The bond distances between ruthenium and the central pyridyl nitrogen of the PYA pincer ligand ($\text{Ru-N2} = 1.961(3)$ Å and $1.9589(19)$ Å in **1** and **2a**, respectively) are substantially shorter compared to the Ru-N_{PYA} bonds (Ru-N1/3 in the $2.102\text{--}2.134$ Å range) because of the compressed geometry of the pincer ligands due to the small bite angle (Table 1). In both complexes, the Ru-N4 bond to the in-plane MeCN ligand is slightly longer ($\text{Ru-N4} = 2.034(3)$ Å and $2.056(2)$ Å in **1** and **2a**, respectively) than the $\text{Ru-N}_{\text{MeCN}}$ bond of the axially coordinated MeCN ligands (Ru-N5/6 between $2.008(3)$ and $2.024(2)$ Å). Whereas the *p*-PYA pincer ligand precursor **L1** (Fig. S1) reveals a completely planar geometry, similar to the previously reported structure of its iodide analogue,⁵³ the PYA heterocycles in the ruthenium complexes are substantially twisted out of the plane of the central pyridine ring by 39.3° and 40.5° in complex **1** and by 41.8° and 34.9° in complex **2a**. This large dihedral angle indicates a low π contribution to the $\text{N}_{\text{PYA}}\text{--C}_{\text{pyridyl}}$ bond and hence little conjugation between the PYA heterocycle and the metal-bound nitrogen. Accordingly, the amide nitrogen is predominantly anionic and π -basic as depicted in the zwitterionic limiting resonance structure **A** (*cf* Scheme 1).

A closer look at the bond length alterations within the PYA systems allows for comparison of the mesomeric flexibility of the PYA ligands (Table 1) which is particularly interesting for complex **1** since the *p*-PYA ligand features two strongly diverting limiting resonance structures (zwitterionic aromatic *vs.* neutral diene, *cf* Scheme 1). Complex **1** shows distinctly shorter bond distances for $\text{C}_\alpha\text{--C}_\beta$ compared to $\text{C}_\beta\text{--C}_\gamma$ ($1.351(7)$ Å *vs.* $1.400(7)$ Å) thus indicating a pronounced diene character (resonance form **A** in Scheme 1). In contrast, the ligand **L1** shows an aromatic structure with only 0.026 Å difference between $\text{C}_\alpha\text{--C}_\beta$ and $\text{C}_\beta\text{--C}_\gamma$. In the *m*-PYA pincer ligand of complex **2a**, the bond length alteration is even smaller (less than 0.02 Å) which is

in good agreement with a predominantly zwitterionic resonance structure and an aromatic PYA heterocycle. This divergence demonstrates the adaptiveness of the *p*-PYA ligand and agrees with solution NMR data, supporting a formally anionic and stronger π -basic metal-bound nitrogen of the *m*-PYA unit.

Table 1. Selected bond lengths (Å) and angles (deg) for ligand **L1** and complexes **1** and **2a**

	L1	1^a	2a^a
Ru1–N1	-	2.102(3)	2.1064(19)
Ru1–N2	-	1.961(3)	1.9589(19)
Ru1–N3	-	2.134(3)	2.1137(18)
Ru1–N4	-	2.034(4)	2.056(2)
Ru1–N5	-	2.008(4)	2.010(2)
Ru1–N6	-	2.016(4)	2.024(2)
N–C $_{\alpha}$ ^b (N7–C2, N7–C6)	1.341(4)	1.335(8)	1.345(3)
C $_{\alpha}$ –C $_{\beta}$ ^b (C2–C3, C5–C6)	1.367(4)	1.351(7)	1.374(4)
C $_{\beta}$ –C $_{\gamma}$ ^b (C3–C4, C4–C5)	1.393(4)	1.400(7)	1.393(4)
N1–Ru1–N3	-	157.82(14)	157.55(8)
θ PYA-pyr ^c	0	39.3, 40.5	34.9, 41.8

^aFor complexes **1** and **2a** the disordered pyridylic ring was not taken into account; ^b average of two bonds; ^c dihedral angle θ between the PYA heterocycles and the N–C=O amide plane.

Preliminary catalytic evaluation. Both complexes were tested as catalysts (1 mol%) in transfer hydrogenation of benzophenone under standard conditions,⁵⁴ *i.e.* using *i*PrOH as hydrogen source under basic conditions (10 mol% KOH) at reflux temperature and under aerobic conditions. While the *p*-PYA complex **1** was essentially inactive and reached less than 5% conversion after 6 h, the *m*-PYA complex **2a** showed appreciable catalytic activity with 97% conversion after 2 h (Fig. 2).

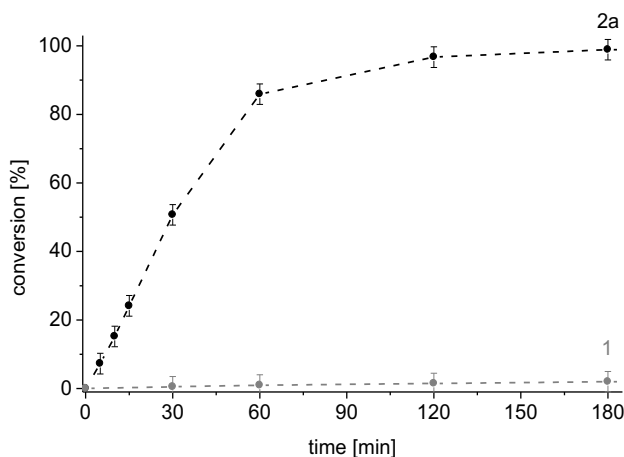


Figure 2. Time-conversion profiles for the transfer hydrogenation of benzophenone in *i*PrOH and KOH (10 mol%) with complex **1** (grey) and complex **2a** (black; both at 1 mol%).

To better understand their radically different catalytic behavior, the two complexes were investigated electrochemically using cyclic voltammetry. Both complexes showed two reversible oxidation processes, which were assigned to a consecutive oxidation of the ruthenium center from +II to +III and then to +IV (Fig. 3, Table 2). The *p*-PYA pincer ligand in complex **1** induces higher oxidation potentials ($E_{1/2} = +0.78$ V for Ru^{II/III} and +1.95 V for Ru^{III/IV}, all potentials *vs.* SSCE) than the *m*-PYA ligand in complex **2** ($E_{1/2} = +0.67$ V and +1.85 V). This 100 mV shift is in agreement with stronger electron donor properties of the *m*-PYA ligand, which can be rationalized by the more pronounced zwitterionic resonance structure contribution, and the low relevance of a π -acidic imine-type neutral structures (*cf* Scheme 1). In contrast, the valence isomerization of the *p*-PYA ligand to the imine resonance form in complex **1** reduces the donor properties, and hence this ligand stabilizes lower metal oxidation states, thus entailing higher oxidation potentials. These electrochemical analyses paired with the NMR and solid state studies underline the electronic tunability of bis-PYA pincer ligand without significantly altering of the steric properties.

Table 2. Characteristic electrochemical and photochemical values for complexes **1** and **2a**

	1	2a
$E_{1/2}(\text{Ru}^{\text{II/III}})$ [V] ^a	0.78 (77)	0.67 (75)
$E_{1/2}(\text{Ru}^{\text{III/IV}})$ [V] ^a	1.95 (148)	1.85 (134)
λ_{max} (MLCT) [nm] ^b	412 (8,100); 504 (4,000)	402 (9,100); 476 (2,900)

^a potentials in MeCN *vs.* SSCE at 100 mV·s⁻¹ scan rate using the Fc⁺/Fc couple as standard; $E_{1/2} = +0.43$ V and (*n*Bu₄N)PF₆ as electrolyte; $\Delta E_p = |E_{\text{pc}} - E_{\text{pa}}|$ [mV] in parenthesis. ^b measured in MeCN; molar extinction coefficient ϵ [L·mol⁻¹·cm⁻¹] in parenthesis.

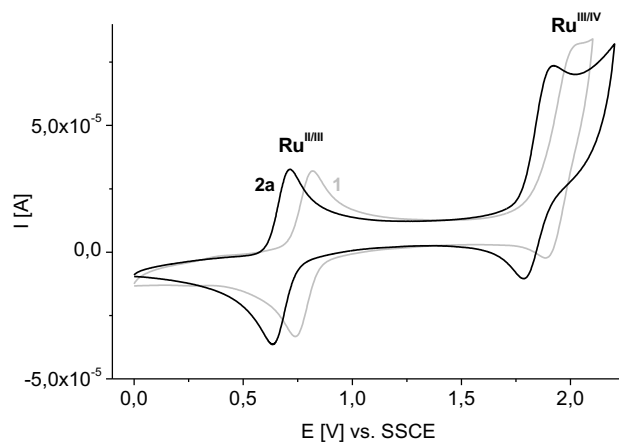


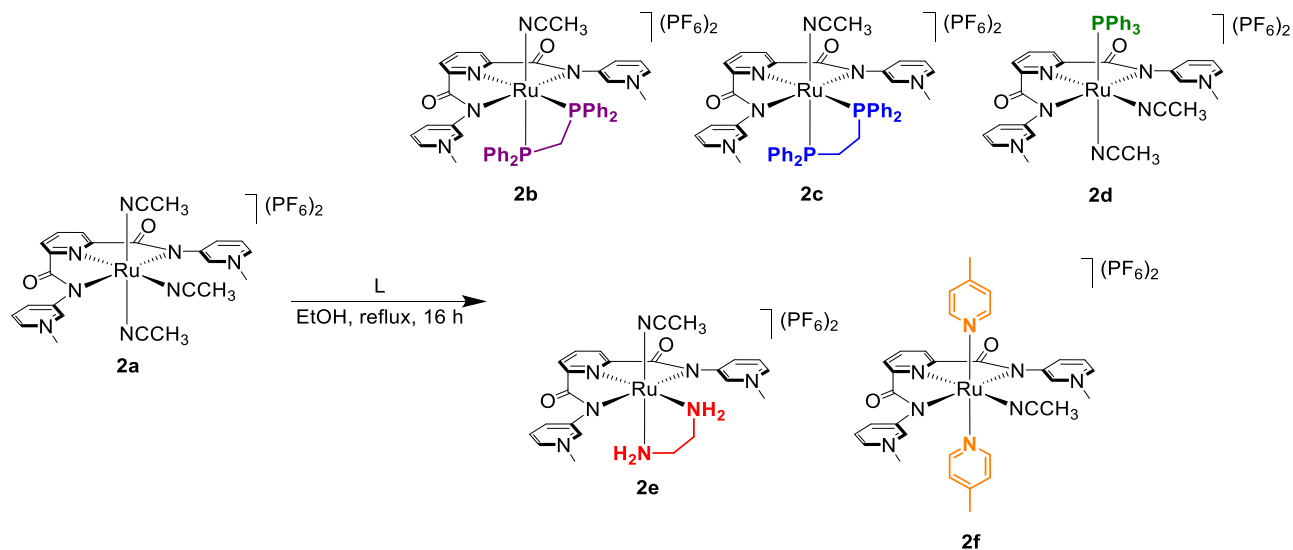
Figure 3. Cyclic voltammometry measurements of complexes **1** (grey) and **2a** (black) in MeCN (potentials vs. SSCE using the Fc⁺/Fc couple as standard; $E_{1/2} = +0.43$ V; (*n*Bu₄N)PF₆ as electrolyte, 100 mV s⁻¹ scan rate).

UV-vis absorption spectra show a similar distinction between the effects of the *m*- and *p*-PYA ligand. The MLCT bands in the visible region of the spectra deriving from metal to ligand d- π^* transitions are useful indicators for the electronic impact of the two ligand types. These bands appear at $\lambda_{\text{max}} = 412$ and 504 nm for complex **1** and are hypsochromically shifted to 402 and 476 nm for complex **2a** (Fig. S4). This shift of λ_{max} corroborates a more pronounced π -acidic diene type structure of the *p*-PYA ligand in complex **1**, which imparts a higher degree of conjugation and electron delocalization and therefore a smaller energy difference between the HOMO d-orbitals (metal-centered) and the ligand-centered unoccupied π^* MOs when compared with the electronic configuration in the zwitterionic *m*-PYA ligand.

All analytic data therefore indicate a significant dependence of the metal properties on the PYA substitution pattern and in particular on the position of the N-Me group. The *m*-PYA pincer ligand exerts stronger donor properties than the more diene-type *p*-PYA pincer ligand in complex **1**, and complex **2a** outperforms the *p*-PYA pincer complex **1** by far in transfer hydrogenation catalysis. Therefore, modification of the ancillary ligands in **2a** has been envisaged as a methodology to improve catalytic activity and to develop 2nd generation transfer hydrogenation catalysts.

Ancillary ligand modulation of complex 2a. Substitution of the MeCN spectator ligands in **2a** was accomplished upon refluxing an EtOH solution of complex **2a** in the presence of extraneous ligands. Based on their distinct steric and electronic impact, a diverse set of ligands was selected, including mono- and bidentate phosphines (diphenylphosphinomethane, dppm; diphenylphosphinoethane dppe; PPh₃), amines (ethylenediamine, en), and imines (4-picoline) to yield complexes **2b-f**, respectively (Scheme 3). While coordination of the bidentate ligands dppm, dppe, and en are unsurprising, it is worth noting that only one

PPh_3 ligand binds to the Ru(*m*-PYA) unit in axial position, even in the presence of a large excess of phosphine. Coordination of only one phosphine is presumably due to steric constraints imparted by the restricted orientation of the N-CH₃ group of the PYA units. In contrast, picoline coordination is sterically less demanding and substitution from **2a** afforded exclusively complex **2f** with two picoline ligands in mutual *trans* position.



Scheme 3. Synthesis of second-generation (*m*-PYA) pincer Ru complexes **2b-f**.

The formation of complexes **2b-f** was confirmed by ¹H NMR, ¹³C{¹H} NMR and ³¹P{¹H} NMR spectroscopy. The spectra of complexes **2b-d** feature the expected new proton resonances in the aromatic region integrating to 20 and 15 H, respectively. In addition, the singlet due to the C2-bound hydrogen of the PYA ligand shifts diagnostically upfield upon phosphine coordination from $\delta_{\text{H}} = 9.07$ in **2a** to $\delta_{\text{H}} \approx 7.7$ in **2b** and **2c**, and less upfield to $\delta_{\text{H}} = 8.33$ in the monophosphine complex **2d**. The limited steric flexibility of the dppe ligand induces a lower symmetry for complex **2c**, as demonstrated by the appearance of two distinct singlets for the C2-H protons of each PYA unit in the ¹H NMR spectrum at $\delta_{\text{H}} = 7.75$ and 7.73 . The *cis*-coordinating dppe ligand appears as AB doublets in the ³¹P{¹H} NMR spectrum at $\delta_{\text{P}} = 0.1$ and -3.2 ($^2J_{\text{PP}} = 57.8$ Hz) for **2b**, and as AX doublet at $\delta_{\text{P}} = 66.2$ and 54.3 ($^2J_{\text{PP}} = 13.8$ Hz) for **2c**. Coordination of only one PPh₃ in complex **2d** was identified by a singlet at $\delta_{\text{P}} = 51.6$ and a 1:2 integral ratio with the highfield PF₆⁻ resonance at $\delta_{\text{P}} = -144.6$ (septett, $^1J_{\text{PF}} = 707$ Hz).

Complexes **2e** and **2f** with nitrogen-containing ancillary ligands showed the signals expected due to the newly bound en and picoline ligands in the aliphatic and aromatic region, respectively. For example, the picoline resonances of complex **2f** appear as two characteristic doublets ($\delta_{\text{H}} = 7.69$ and 7.06 , $^3J_{\text{HH}} = 6.6$ Hz) and integrated for two symmetry-related and hence mutually *trans* coordinated ligands. Interestingly, the C2–H proton resonance is less shifted upon en coordination ($\delta_{\text{H}} = 8.48$) than in the phosphine complexes, and it is unchanged in the picoline complex **2f** at ($\delta_{\text{H}} = 9.08$, *cf* 9.07 for **2a**). The C2–H proton resonance of the *m*-PYA unit therefore is a sensitive probe for the stereoelectronic impact of the ancillary ligands.

Modification of the ancillary ligands also had a marked influence on the lability of the residual MeCN ligands. While NMR spectra in deuterated MeCN or DMSO did not indicate any substitution of this ligand in complexes with N-donor ligands (**2a**, **2e**, and **2f**), phosphine coordination in complexes **2b–d** induced rapid ligand exchange in both solvents and no coordinated MeCN was observed in the ^1H NMR spectrum of the dppx complexes **2b** and **2c**. For complex **2d** only one resonance for coordinated MeCN was observed ($\delta_{\text{H}} = 2.98$ in DMSO- d_6 and 2.67 in MeCN- d_3 , respectively), which decreased in a zero-order reaction and completely disappeared after 24 h (Fig. S8, S9). In non-coordinating CD_2Cl_2 both coordinated MeCN ligands were observed and resonant at $\delta_{\text{H}} = 2.26$ and 2.54 (Fig. S10).

1D NOESY measurements of **2d** in CD_2Cl_2 and MeCN- d_3 were carried out to unambiguously assign the position of the MeCN ligands and to investigate the rotation dynamics of the PYA units in solution (Fig. S11–S15). Upon saturation of the MeCN proton resonance at $\delta_{\text{H}} = 2.54$ in CD_2Cl_2 solution, spin-spin coupling to the N–CH₃ protons of the PYA unit ($\delta_{\text{H}} = 4.31$) and to the PPh₃ protons ($\delta_{\text{H}} = 6.8$ – 6.9 and 7.0 – 7.1) was observed, suggesting an equatorial position of this MeCN ligand and a *cis* relationship with PPh₃. In contrast, saturation of the MeCN resonance at $\delta_{\text{H}} = 2.26$ did not show any interaction with the PPh₃ protons nor the N–CH₃ group, which is in agreement with an axial position with respect to the pincer ligand plane (*viz.* *trans* to PPh₃). In MeCN- d_3 , one MeCN ligand is rapidly exchanging and only one NCCH₃ resonance was observed (*vide supra*). Saturation of this resonance ($\delta_{\text{H}} = 2.67$) revealed an NOE with the PPh₃ protons, indicating that the axial MeCN ligand is significantly more labile, in agreement with the higher *trans* effect of PPh₃ vs the pyridyl donor site⁵⁵ of the pincer ligand.

Irrespective of the solvent (CD_2Cl_2 or MeCN- d_3), NOEs were also observed between the equatorial MeCN proton resonances and three of the four protons of the pyridylidene heterocycle (H², H⁴, and H⁵). These interactions indicate substantial wagging of the PYA unit about the exocyclic C–N_{PYA} bond and suggest single bond character of this bond. Such a conclusion is corroborating the preponderance of the zwitterionic PYA form (C in Scheme 1) and provides another indication for a formally anionic and π -basic PYA nitrogen donor site in complex **2a**.

Interestingly, the different degrees of lability of the MeCN ligand are also reflected in the HR-MS data of complexes **2b–f**. The phosphine complexes **2b–d** all show a M^+ signal resulting from dissociation of a PF_6^- anion and all MeCN ligands ($m/z = 978.1259$ for $[2b-MeCN-PF_6]^+$, 992.1430 for $[2c-MeCN-PF_6]^+$, and 856.0985 for $[2d-2MeCN-PF_6]^+$) in excellent agreement with the calculated values (978.1259 , 992.1415 , and 856.0973 , respectively). In contrast, the N-donor complexes ionized only via loss of the PF_6^- anion, and the mother ion included the coordinated MeCN ligand ($m/z = 695.1032$ for $[2e-PF_6]^+$ and 821.1528 for $[2f-PF_6]^+$).

Crystallographic analysis. The structures of complexes **2b–d** and **2f** were unequivocally confirmed by single crystal X-ray diffraction analysis. All complexes show a distorted octahedral ruthenium center with the *m*-PYA pincer ligand in a meridional coordination mode (Fig. 4). The bite angle of the pincer ligand $N1-Ru-N3$ decreases from 157.6° in the solvento complex **2a** to 155.8° in **2d** with one PPh_3 ligand and even further to 152.6° and 152.9° in the bidentate dppx complexes **2b** and **2c** (Table 2). The phenyl rings of the dppx ligands and the PYA heterocycle are oriented in a parallel manner, indicative of π -stacking interactions. These interactions lead to large twist of the PYA heterocycle out of the pyridylamide plane with dihedral angles between $61-82^\circ$ in complexes **2b** and **2c** compared to less than 42° in complexes **2a**, **2d** and **2f**. Another distinctive feature is the expected higher *trans* influence of the phosphine ligand compared to pyridine in these complexes as demonstrated by the lengthening $Ru-N_{pyr}$ and $Ru-N_{MeCN}$ bonds. This higher *trans* influence correlates here also with a higher *trans* effect, as noted for the fast substitution of the MeCN ligand *trans* to a phosphine in complexes **2b–d**.

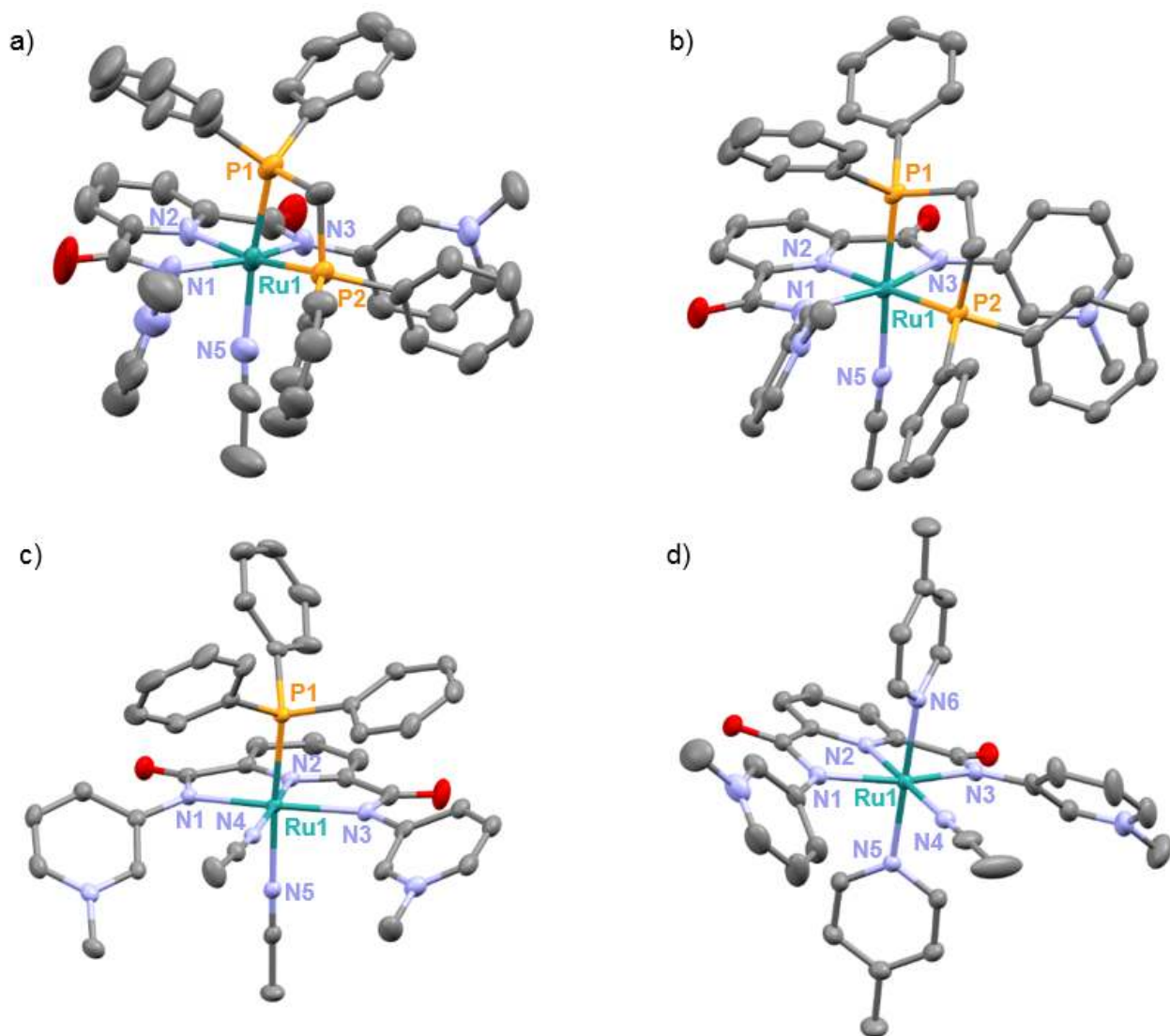


Figure 4. ORTEP representations of the complex cations of **2b** (a), **2c** (b), **2d** (c) and **2f** (d); all ellipsoids at 50% probability, H atoms, non-coordinating PF_6^- anions, co-crystallized solvent molecules, and conformational disorder of methyl-pyridinium rings omitted for clarity.

Table 3. Selected bond lengths (\AA) and angles (deg) for complexes **2a–d** and **2f**

	2a ($L_{\text{ax}} = \text{N5}$)	2b ($L_{\text{ax}} = \text{P1}$)	2c ($L_{\text{ax}} = \text{P1}$)	2d ($L_{\text{ax}} = \text{P1}$)	2f ($L_{\text{ax}} = \text{N5}$)
Ru–N1	2.1064(19)	2.114(5)	2.161(3)	2.147(2)	2.1208(18)
Ru–N2	1.9589(19)	2.034(5)	2.047(3)	1.977(2)	1.953(2)
Ru–N3	2.1137(18)	2.134(4)	2.146(3)	2.136(2)	2.1208(18)
Ru–N4 or Ru–P2	2.056(2)	2.2951(15)	2.3209(10)	2.050(2)	2.055(3)
Ru–N5	2.010(2)	2.102(5)	2.118(3)	2.096(2)	2.0910(18)

Ru–L _{ax}	2.024(2)	2.2642(16)	2.2802(11)	2.3271(6)	2.0910(18)
N1–Ru–N3	157.55(8)	152.6(2)	152.85(12)	155.79(8)	157.06(10)
θ PYA–pyr ^a	34.9, 41.8	76.9, 79.3	61.7, 81.9	31.6, 40.2	41.3, 41.3

^adihedral angle θ between the PYA heterocycles and the pyridylamide plane.

Electrochemical and UV-vis spectroscopic analysis. Electrochemical measurements and spectroscopic data suggest a strong influence of the different spectator ligands on the electronic properties of the Ru(II) metal center. Cyclic voltammetry in MeCN shows for all complexes a reversible oxidation in the +0.2 to +1.0 V range which was attributed to a metal-centered Ru^{II/III} redox process.⁵⁶

When comparing the half-wave potentials (Fig. 5, Table S1) a trend emerges that correlates with the donor properties of the ancillary ligand. The oxidation potentials increase in the sequence **2e** (0.26 V) < **2f** (0.46 V) < **2a** (0.67 V) < **2d** (0.79 V) < **2c** (0.86 V) \approx **2b** (0.88 V; all potentials vs SSCE), in agreement with the hardness of the ligand setting, which decreases in the order of en (**2e**) > pyr (**2f**) > RCN (**2a**) > PR₃ (**2d**). Exchange of another MeCN ligand by a second phosphine (**2b**, **2c**) further reduces the electron density at the metal center and hence increases the potential needed to reach the oxidized Ru^{III} state. Hence, the ancillary ligands allow the electronic properties of the ruthenium center to be tailored over a substantial potential range.

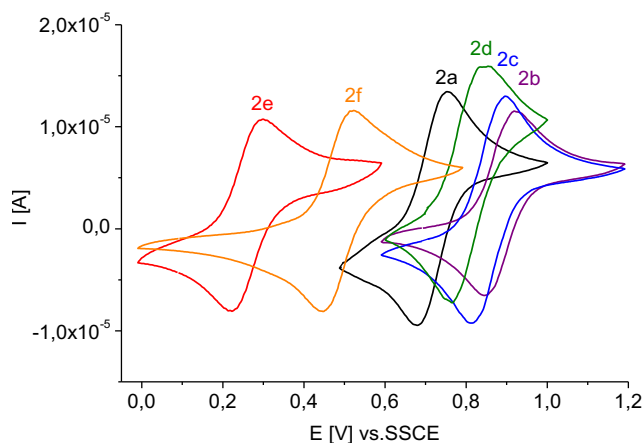


Figure 5. Cyclic voltammometry measurements of the *m*-PYA Ru(II) complex variations **2a** (black, L = MeCN), **2b** (purple, L = dppe), **2c** (blue, L = dppe), **2d** (green, L = PPh₃), **2e** (red, L = en) and **2f** (orange, L = 4-picoline) in MeCN showing the reversible redox processes for the Ru^{II/III} transition (potentials vs. SSCE using the Fc⁺/Fc couple as standard; $E_{1/2} = +0.43$ V; *n*Bu₄NPF₆ as supporting electrolyte, 100 mV s⁻¹ scan rate).

Photospectroscopic measurements of the complexes show an absorption in the 350–450 nm range that was assigned to a d– π^* MLCT band (Fig. S5). The absorption maximum λ_{max} of this band is strongly dependent

on the ancillary ligand and shifts to higher energy as the ligand hardness is reduced following the sequence **2e** (456 nm) > **2f** (437 nm) > **2a** (402 nm) > **2d** (390 nm) > **2b** (367 nm) \approx **2c** (360 nm). This sequence is identical to the order of redox potentials established by electrochemical measurements and hence supports the notion that the electronic properties of these *m*-PYA pincer ruthenium complexes can be tailored over a broad range. Interestingly, a plot of the absorption maxima (λ_{max}) vs the redox potentials ($E_{1/2}$) is linear (Fig. 6), indicative of a direct correlation. Since the Ru^{II/III} redox potentials are predominantly affected by the metal 4d orbital energy of the HOMO, the linear correlation with λ_{max} implies that the energy of the LUMO remains constant. It therefore follows that for all investigated complexes **2a–f**, the LUMO is centered on the *m*-PYA pincer ligand. Considering the π -basic nature of the amide donor sites of the PYA pincer ligand, these data suggest the LUMO to be largely localized on the central pyridyl ring. Hence this pincer ligand is behaving as a π acid, qualitatively similar to terpyridine.

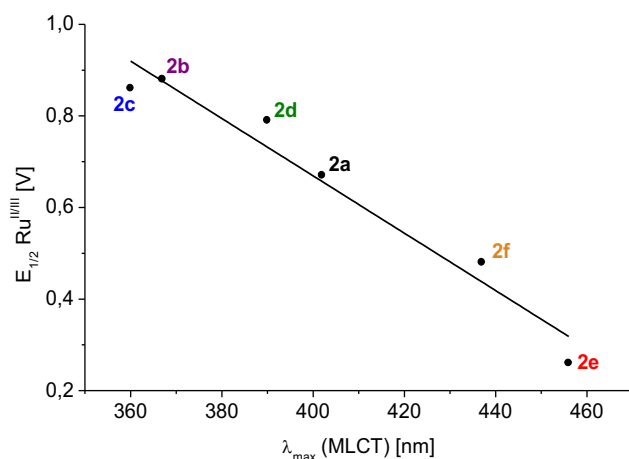


Figure 6. Linear correlation of the Ru^{II/III} redox potentials $E_{1/2}$ with the maximum absorption λ_{max} of the MLCT process for the *m*-PYA pincer ruthenium complexes **2a–f** ($R^2 = 0.95$).

Catalytic transfer hydrogenation activity of complexes 2a–f. The 2nd generation *m*-PYA pincer ruthenium(II) complexes **2b–f** were tested as catalyst precursors for the transfer hydrogenation of benzophenone in *i*PrOH under basic conditions and compared to **2a**. At 1 mol% ruthenium loading, the complexes with ancillary phosphine ligands **2b–d** displayed the best performance of the series and reached turnover frequencies at 50% conversion (TOF_{50}) up to 430 h⁻¹ (Fig. 7, Table 4, entries 2–4), which is a threefold increase compared to complex **2a** with MeCN ancillary ligands ($\text{TOF}_{50} = 100$ h⁻¹; entry 1). Complexes **2e** and **2f** with en and pyridine ancillary ligands, respectively, were considerably less active (entries 8, 9). While complex **2f** reached almost 70% conversion after 2 h ($\text{TOF}_{50} = 40$ h⁻¹), the en-containing complex **2e** was essentially inactive and reached a modest 20% conversion after 2 h. This substantial variation of catalytic activity in complexes **2a–f** demonstrates the tunability of the *m*-PYA pincer ruthenium unit.

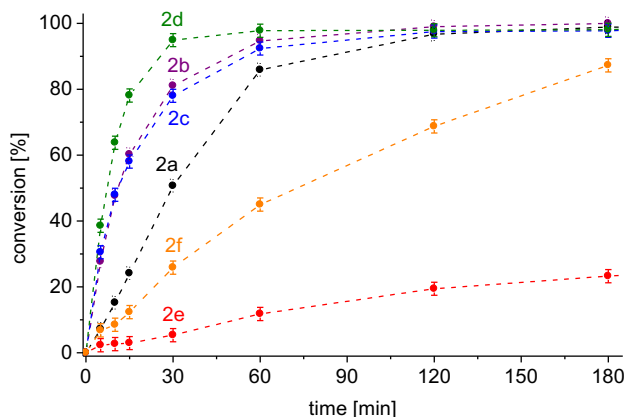
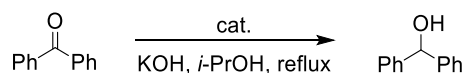


Figure 7. Time-conversion profile for *m*-PYA ruthenium complexes with variable ancillary ligands in the transfer hydrogenation of benzophenone: **2a** (black), **2b** (purple), **2c** (blue), **2d** (green), **2e** (red) and **2f** (orange).

Table 4. Catalytic activity of complexes **1** and **2a–f** in transfer hydrogenation of benzophenone ^a



entry	cat.	yield (%) ^b			TOF ₅₀ (h ⁻¹)
		0.25 h	0.5 h	2 h	
2	2a	24	51	97	100
3	2b	60	81	99	300
4	2c	58	78	98	300
5	2d	78	95	98	430
6 ^c	2d	18	26	44	150
7 ^d	2d	<2	<2	<2	-
8	2e	3	5	20	-
9	2f	12	26	69	40

^a General reaction conditions: benzophenone (1 mmol), KOH (0.1 mmol, 10 mol%), [Ru] (0.01 mmol, 1 mol%), *i*PrOH (5 mL), reflux temperature. ^b determined by GC using hexadecane as internal standard and averaged over at least two runs, conversions correspond with yields. ^c [Ru] (0.001 mmol, 0.1 mol%). ^d Without base

When the most active catalyst **2d** was evaluated at lower catalyst loadings of 0.1 mol%, catalytic activity was preserved with a TOF_{50%} of 150 h⁻¹ (entry 6), though considerably longer reaction times were required to reach high conversion (87% after 24 h, corresponding to 870 turnovers). The presence of a base is essential, as under base-free conditions no substrate was converted (entry 7).

While the enhanced catalytic activity of the *m*-PYA pincer complex in comparison to the *p*-PYA analogue was attributed to the stronger donor properties of the mesoionic PYA ligand sites in complex **2**, such arguments based on electron donor ability fall short to rationalize the observed catalytic activity trend for

2a–f. The complexes with the highest redox potential, *i.e.* the phosphine complexes with the least electron-donating ligand set, show the highest catalytic activity. In fact, the ligand donor properties correlate inversely with the catalytic activity. A more plausible rationale for the high catalytic activity of complexes **2b–d** therefore invokes the high *trans* effect of the phosphine ligand, which labilizes in particular the MeCN ligand *trans* to the phosphine (*cf* NMR studies above). According to such a model, substrate coordination and presumably also product release is facilitated in these complexes. Steric congestion imparted by the equatorial phosphine in the diphosphine complexes **2b** and **2c** may account for the slightly lower activity of these complexes when compared to the monophosphine complex **2d**.

Catalytic transfer hydrogenation studies with 2d as the most active complex. Based on its high activity, complex **2d** was used to investigate catalyst longevity and a brief substrate scope. The robustness of the catalytically active species was probed by increasing the substrate/catalyst (S/C) ratio. At a 1,000:1 S/C ratio, the reaction is considerably slower and 24 h rather than 30 min are required to reach synthetically useful conversions. Lowering the catalyst concentration from 1 mM to 0.1 mM (*cf* entry 6 in Table 3) had the same effect as increasing the substrate concentration from 0.1 M to 1 M, suggesting that the intrinsic stability of the catalytic species is limiting the longevity and not potential impurities of the solvent or aerobic oxidative catalyst degradation. In an attempt to preserve the high turnover frequency observed when applying a 100:1 S/C ratio, a further experiment was carried out in which 100 equiv. benzophenone were added consecutively each 20 min. After 10 additions, the same 1,000:1 S/C ratio was reached. A 20 min interval was selected because after this time, the 100:1 S/C run shows high but not full conversion (*cf* entry 5, Table 3). This situation ensures that the catalyst is still active.

The conversion profile of this run with stepwise addition of substrate reveals a gradual decrease of catalytic activity as shown by the reduction of turnover numbers (TONs) within each 20 min segment, from 78 in the first segment to a modest 10 in the last segment (Fig. 8). Interestingly however, after 8 h, the conversion is essentially identical to runs which started directly at a 1,000:1 S/C ratio (TONs of 750 ±50). This result implies that catalytic activity resumes after the additions are complete (*i.e.* after 200 min) and that the repeated sampling and substrate addition is inhibiting catalytic turnover. Inhibition has been attributed to a reversible deactivation of the catalytically active species by oxygen. Such deactivation is promoted by the repetitive opening of the reaction vessel for sampling and is reversed by solution degassing through reflux. Support for such a conclusion was obtained from a run in which only substrate was added but no samples were taken to determine conversion. After 210 min, this run reached much higher conversion than when sampling after each substrate addition (520 vs 420 TON, compare to 710 TON of a sample starting at 1,000:1 ratio without any sampling or substrate addition). However, final conversions are identical with previous runs, which is in agreement with a reversible deactivation of the catalytic species. Moreover, a catalytic run

at 1,000:1 ratio under strict exclusion of air featured the highest catalytic activity, reaching a TOF_{50} of 4,000 h^{-1} (7.5 min for 50% conversion), almost full conversion after 30 min, and a final TON of 990. These experiments provide strong support for reversible catalyst inhibition by oxygen, in agreement with the formation of a sensitive hydride species with sufficiently long life time.⁵⁷ Moreover, the regeneration of the active species under reflux conditions indicates a catalytic species that is molecularly well-defined and homogeneously operating.

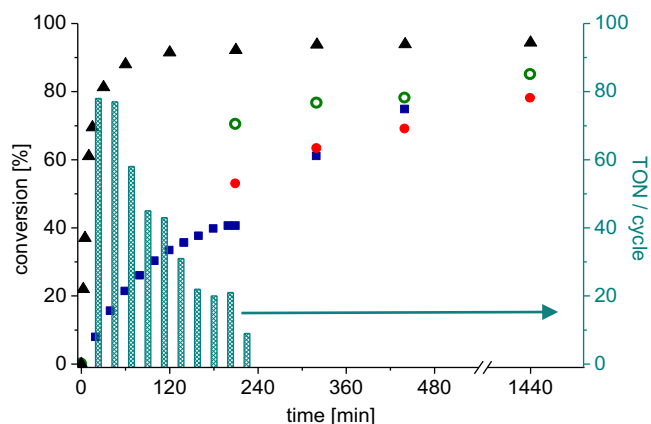
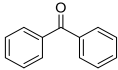
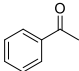
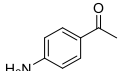
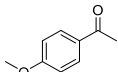
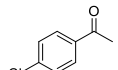
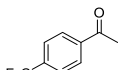
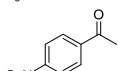
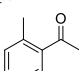
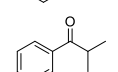
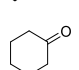
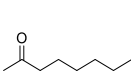
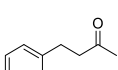
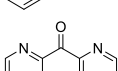
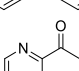
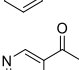
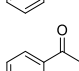
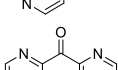
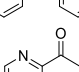


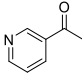
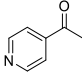
Figure 8. Conversion and TON profiles for the transfer hydrogenation of benzophenone with complex **2d** in *i*PrOH under different conditions: ■ stepwise addition of 10x 100 equiv. substrate every 20 min (sampling every 20 min); pillars show the TON for each of those 10 cycles; ● stepwise addition of 100 equiv. substrate every 20 min (with no sampling before 210 min); ○ S/C 1000:1 from onset under aerobic conditions; ▲ S/C 1000:1 from onset under N_2 atmosphere; conversions are plotted based on the final 1000:1 S/C ratio.

A preliminary evaluation of the substrate scope of complex **2d** involved diaryl, aryl-alkyl, and dialkyl ketones, which were hydrogenated with high conversion, including open chain and cyclic aliphatic ketones (see Fig. S16, S17 for time-conversion profiles). Transfer hydrogenation of (substituted) acetophenones under aerobic conditions proceeded at rates that are comparable to those observed for the reduction of benzophenone (entries 1–8). No direct electronic effect was observed and electron withdrawing (*e.g.* $-\text{CF}_3$, entry 6) as well as electron-donating groups ($-\text{OMe}$, entry 4) were converted at similar rates, though slightly slower in comparison to unsubstituted acetophenone (entry 2). Nitrogen-containing substituents were incompatible with the catalyst and both nitro as well as amine groups inhibited transfer hydrogenation significantly, presumably due to amine coordination to the active site. Remarkably, sterically shielded 2-methylacetophenone was hydrogenated faster than the unshielded parent substrate and >90% conversion was achieved already after 15 min (entry 8). Steric shielding of the alkyl side of acetophenone led to decreased catalytic rates and isobutyrophenone was hydrogenated only to 46% within the same reaction period (entry 9). Cyclohexanone as a representative cyclic aliphatic ketone was converted very rapidly and essentially complete conversion was noted after 15 min (entry 10). In contrast, open chain aliphatic ketones

such as 2-octanone and 4-phenyl-2-butanone react slightly slower than acetophenone and up to 2 h are required to reach maximum conversion (entries 11,12).

Table 5. Substrate scope of complex **2d** in catalytic transfer hydrogenation ^a

entry	substrate	yield (%) ^b			TOF ₅₀ (h ⁻¹)
		0.25 h	0.5 h	2 h	
1		78	95	98	430
2		82	98	>99	350
3		26	36	49	20
4		73	85	90	450
5		71	95	>99	290
6		65	88	>99	300
7		<2	<2	<2	-
8		91	99	>99	550
9		46	57	87	150
10		99	>99	>99	490
11		62	80	96	310
12		71	92	>99	360
13		40	46	58	60
14		<2	3	5	-
15		15	18	28	-
16		11	14	21	-
17 ^c		82	>99	>99	320
18 ^c		44	87	>99	180

19 ^c		11	21	68	40
20 ^c		9	14	38	20

^a General reaction conditions: substrate (1 mmol), KOH (0.1 mmol, 10 mol%), **2d** (0.01 mmol, 1 mol%), *i*PrOH (5 mL), reflux temperature, aerobic conditions; ^b determined by ¹H NMR spectroscopy using anisole or hexamethylbenzene as internal standard, conversions correspond to yields, calculated as an average of at least two runs; ^c complex **2c** (0.01 mmol, 1 mol%) as catalyst.

Pyridyl-containing ketones are generally challenging substrates for transfer hydrogenation because the pyridyl group favorably competes with the carbonyl group for coordination to late transition metals and often inhibits substrate conversion (*cf* also entries 3,7). Indeed, conversion of di(2-pyridyl)ketone and the different acetylpyridines with complex **2d** was only moderate to low (entries 13–16). Inspection of the time-conversion profiles reveals some interesting insights (Fig. 9). The initial conversion rates are substrate-dependent and therefore point to substrate inhibition of the catalytic species. By far the lowest activity was noted for 2-acetylpyridine (<2 TON after 15 min, entry 14), which is attributed to a higher stability of *N*-coordination of the substrate supported by *N,O*-bidentate chelation. Similar chelation is sterically disfavored in 3- and 4-acetyl pyridine and hence, these substrates are converted faster (entries 15,16). While dipyridylketone may chelate in a similar way as 2-acetylpyridine, *N,O*-bidentate bonding is surmised to be weakened due to the low electron density of the carbonyl group because of the two pyridyl substituents, and turnover frequencies are considerably higher (40 TON after 15 min, entry 13). In agreement with such a model, conversion of this substrate drops markedly after about 40% conversion, which is attributed to product inhibition as the hydrogenated product is a stronger chelate than the substrate (more basic pyridyl unit and alkoxide as stronger donor than ketone).

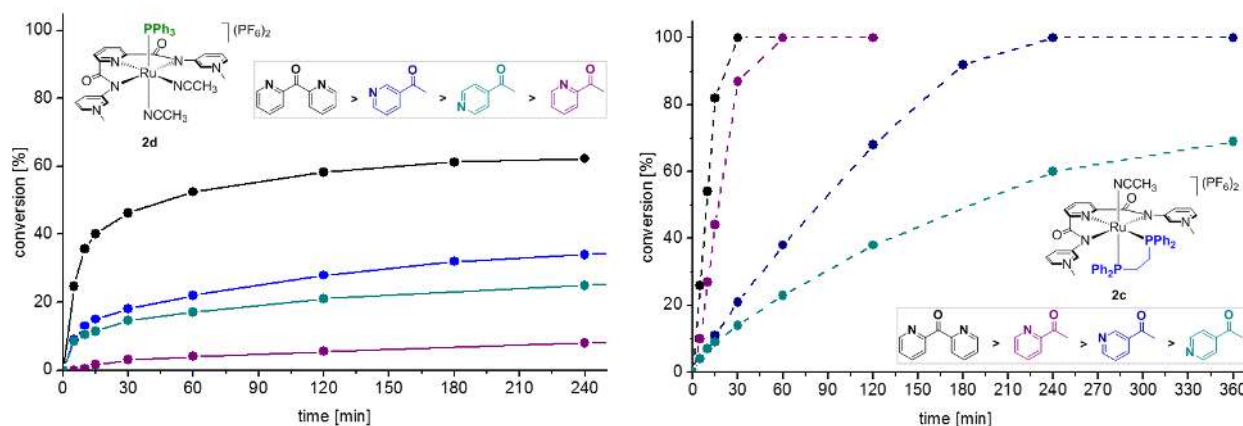
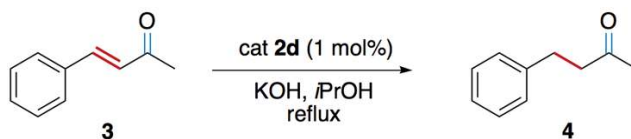


Figure 9. Time-conversion profiles for the transfer hydrogenation of pyridyl-substituted ketones with monophosphine complex **2d** (left, solid lines) and diphosphine complex **2c** (right, dashed lines). Reaction conditions as indicated in Table 5.

Based on these considerations, we used complex **2c** which has only one substitution-labile site for substrate coordination due to the bidentate dppe ligand (entries 17–20). This complex configuration prevents chelation of the substrate or product. Indeed, conversion of 2-acetylpyridine is substantially enhanced, reaching essentially full conversion already after 30 min (entry 18). Similarly, inhibition with 2-pyridylketone or its product dipyridylmethanol is suppressed and transfer hydrogenation is complete within 15 min (entry 17). The effect of the dppe ancillary ligand is less pronounced for 3- and 4-acetylpyridine (entries 19,20, essentially complete conversion after 4 and 24 h, respectively), presumably because the pyridine coordination site is sterically less protected as the acetyl group is in more remote position. Hence, engineering of the ancillary ligand allows to tailor the pincer PYA ruthenium complexes for the transformation of challenging substrates.

The activity of complex **2d** towards α,β -unsaturated ketones was evaluated using methyl cinnamylketone **3** as substrate. Transfer hydrogenation produced selectively the saturated ketone 4-phenyl-2-butanone **4** as the only product within 30 min and the reaction composition did not alter upon extending the reaction time to several hours (Scheme 4). This outcome is distinct from most other transfer hydrogenation catalysts which either produce mixtures of products from hydrogenation of the C=C bond, the ketone, or both, typically yielding the fully saturated product.^{58,59,60} For example Noyori-type catalysts are known for their carbonyl-selective hydrogenation of α,β -unsaturated ketones.⁶¹ Only very few catalytic systems are known that selectively reduce only the C=C bond in such Michael systems, requiring either precious metals,⁶² or peculiar reaction conditions such as ionic liquids.⁶³



Scheme 4. Selective olefin transfer hydrogenation of methyl cinnamylketone **3** with complex **2d** producing the saturated ketone **4** as the exclusive product.

The NMR spectra of samples taken at different time intervals only reveal the characteristic resonances of the product and the starting material, but no trace of an allyl alcohol product that would result from ketone reduction (Fig. S18). These observations suggest that either double bond isomerization is very fast, or that the catalyst is selectively reducing the conjugated C=C bond of the substrate. The selectivity of this reduction is remarkable when considering that the product ketone is per se a suitable substrate that is converted to completion in a separate catalytic run within one hour (Table 5, entry 12; Fig. S19). The selective olefin hydrogenation of **3** therefore implies that olefin reduction of methyl cinnamylketone

deactivates the catalytically active species. This hypothesis was verified by running a catalytic experiment using initially methyl cinnamylketone as a substrate followed by addition of acetophenone (1 molequiv.) after 30 min. Conversion of acetophenone was negligible, reaching just 5% after 6 h (Fig. S20; *cf* full conversion after 0.5 h in a separate run, Table 5 entry 2). Several attempts, to characterize the deactivated species have been unsuccessful so far, which prevents the postulation of a plausible rationale for this exquisite selectivity in the reduction of this unsaturated ketone. Similar reactivity patterns were observed with related α,β -unsaturated ketones such as *trans*-chalcone, while 1-phenyl-2-buten-3-one was fully reduced to the saturated alcohol. However, with both substrates, considerable amounts of side products were formed due to oxidative C=C bond cleavage (see SI for details).

Conclusions

Here we have designed and exploited the properties of a new *N,N,N*-tridentate pincer ligand containing zwitterionic *m*-PYA chelating groups. The distinct structural and electronic properties of these chelating groups compared to *p*-PYA systems with more pronounced valence isomerism induce significant catalytic activity of the ruthenium complexes in transfer hydrogenation, in contrast to the *p*-PYA analogue which was catalytically silent. Substitution of the ancillary ligands of the $[\text{Ru}(\text{N}^{\wedge}\text{N}^{\wedge}\text{N})\text{L}_3]$ complex provides a method to rationally tailor the electron density at the ruthenium(II) center and its catalytic activity. Phosphine ligands increase the catalytic activity substantially, and mechanistic investigations indicate that this enhancement is conveyed by the strong *trans* effect of phosphines and the ensuing lability of the MeCN ligand for facile substrate coordination and product release.

Moreover, the PYA pincer platform imparts stability and provides access to a molecular catalyst with appreciable turnover numbers, and unusual selectivity patterns, as demonstrated with the selective C=C bond hydrogenation in α,β -unsaturated ketones and the efficient transfer hydrogenation of 2-acetylpyridine. Due to the facile synthetic assembly and their unique properties, such PYA pincer systems provide an attractive scaffold for other metals and catalytic processes.

Experimental

General. All reagents were commercially available and used as received. Unless specified otherwise, NMR spectra were recorded at 25 °C on Bruker spectrometers operating at 300 or 400 MHz (^1H NMR), and 100 MHz (^{13}C NMR), respectively. Chemical shifts (δ in ppm, coupling constants J in Hz) were referenced to residual solvent signals (^1H , ^{13}C). Assignments are based on homo- and heteronuclear shift correlation spectroscopy. Purity of bulk samples of the complexes has been established by NMR spectroscopy, and

when possible by elemental analysis. Elemental analyses were performed at DCB Microanalytic Laboratory using a Thermo Scientific Flash 2000 CHNS-O elemental analyzer. High-resolution mass spectrometry was carried out with a Thermo Scientific LTQ Orbitrap XL (ESI-TOF) by the mass spectroscopy group of the Department of Chemistry and Biochemistry, University of Bern, PD Dr. S. Schürch. Gas chromatography measurements were performed on the 7697A Headspace Sampler and 7820A GC System by Agilent Technologies. The UV-1800 from Shimadzu with 1 cm quartz cuvettes was used for the UV/Vis measurements. Cyclic voltammograms were recorded using an Autolab PGSTAT101 from Metrohm in MeCN solutions: 10 ml solvent, 1 mM sample and 100 mM tetrabutylammonium hexafluorophosphate ($n\text{Bu}_4\text{N}$)PF₆ as supporting electrolyte). Solutions were deaerated with argon gas for 10 min prior to each run. The scan rate was 100 mV/s. Redox potentials were measured using a Pt-button working electrode, an Ag/AgCl reference electrode (SSCE) and a Pt-wire auxiliary electrode and are tabulated versus a ferrocene internal standard. The Fc⁺/Fc couple is 0.43 V vs. SSCE in 0.1 M ($n\text{Bu}_4\text{N}$)PF₆ MeCN solutions.⁶⁴

Synthetic procedures

Compound L1: To a suspension of the iodide salt (1.560 g, 2.6 mmol) in MeCN (30 mL) a solution of NH₄PF₆ (2.119 g, 13.0 mmol) in H₂O (60 mL) was added under vigorous stirring. The white suspension was heated to reflux for 5 min, which gave a clear solution. Upon slow cooling to room temperature colourless crystals formed. They were collected by filtration and washed with water and Et₂O and dried under reduced pressure to give **L1** as colourless needle-like crystals (1.564 g, 96%). ¹H NMR (300 MHz, DMSO-*d*₆) δ 11.95 (s, 2H, NH_{amide}), 8.87 (d, ³J_{HH} = 7.4 Hz, 4H, H_{PYA}), 8.56–8.58 (m, 2H, H_{pyr}), 8.49 (d, ³J_{HH} = 7.4 Hz, 4H, H_{PYA}), 8.44–8.50 (m, 1H, H_{pyr}), 4.26 (s, 6H, N–CH₃). ¹³C NMR (101 MHz, DMSO-*d*₆) δ 163.3 (CO), 150.8 (C_{pyr}), 147.2 (C_{pyr}), 146.2 (CH_{pyr}), 141.0 (CH_{pyr}), 127.3 (CH_{pyr}), 116.0 (CH_{pyr}), 46.7 (N–CH₃). ESI MS (CH₃CN) m/z: 494.12 [M – PF₆]⁺, 348.15 [M – 2PF₆ – H]⁺. HR-MS: m/z calculated for C₁₉H₁₉O₂N₅F₆P [M – PF₆]⁺ = 494.1151; found: 494.1175. Elemental Analysis: Anal. calculated for C₁₉H₁₉F₁₂N₅O₂P₂: C: 35.70; H: 3.00; N: 10.95. Found: C: 35.63; H: 3.85; N: 10.69.

Compound L2: This product was prepared according to the same procedure as described for **L1** from the iodide salt X2 (1.808 g, 3.0 mmol) in MeCN (50 mL) and NH₄PF₆ (2.458 g, 15.0 mmol) in H₂O (100 ml), which afforded **L2** as colourless crystals (1.863 g, 97%). ¹H NMR (300 MHz, DMSO-*d*₆) δ 11.67 (s, 2H, NH_{amide}), 9.72 (s, 2H, H_{PYA}), 8.85 (d, ³J_{HH} = 8.6, 2H, H_{PYA}), 8.82 (d, ³J_{HH} = 6.0, 2H, H_{PYA}), 8.53–8.55 (m, 2H, H_{pyr}), 8.43–8.47 (m, 1H, H_{pyr}), 8.23 (dd, ³J_{HH} = 8.6, 6.0 Hz, 2H, H_{PYA}), 4.47 (s, 6H, N–CH₃). ¹³C NMR (101 MHz, DMSO-*d*₆) δ 162.4 (CO), 147.3 (C_{pyr}), 141.1 (CH_{pyr}), 141.0 (CH_{pyr}), 137.9 (C_{pyr}), 136.4 (CH_{pyr}), 135.1 (CH_{pyr}), 127.9 (CH_{pyr}), 126.6 (CH_{pyr}), 48.7 (N–CH₃). ESI MS (CH₃CN) m/z: 494.12 [M – PF₆]⁺, 174.58 [M – 2PF₆]²⁺. Elemental Analysis: Anal. calculated for C₁₉H₁₉F₁₂N₅O₂P₂: C: 35.70; H: 3.00; N: 10.95. Found: C: 35.66; H: 3.00; N: 10.89.

Complex 1: A solution of **L1** (130 mg, 0.20 mmol), $[\text{RuCl}_2(\text{cym})]_2$ (60 mg, 0.10 mmol) and Na_2CO_3 (65 mg, 0.60 mmol) in MeCN (50 mL) was stirred at reflux for 16 h. The reaction mixture changed colour from orange to deep red. After cooling to rt, the reaction mixture was filtered over Celite and the red solution was concentrated under reduced pressure to 5 mL. Addition of Et_2O (100 mL) gave a dark red precipitate which was collected by filtration and redissolved in MeCN (10 mL), filtered over Celite and precipitated again by addition of Et_2O (100 mL). The product was collected by filtration and drying of the residue under reduced pressure yielded the complex as a red-brown powder **1** (157 mg, 91%). ^1H NMR (300 MHz, $\text{DMSO}-d_6$) δ 8.52 (d, $^3J_{\text{HH}} = 7.3$ Hz, 4H, H_{PYA}), 8.19–8.21 (m, 3H, H_{pyr}), 7.91 (d, $^3J_{\text{HH}} = 7.3$ Hz, 4H, H_{PYA}), 4.13 (s, 6H, N– CH_3), 2.76 (s, 3H, NCCH_3), 2.34 (s, 6H, NCCH_3). ^{13}C NMR (101 MHz, $\text{DMSO}-d_6$) δ 170.9 (CO), 164.3 (C_{pyr}), 153.9 (C_{pyr}), 144.1 (CH_{pyr}), 139.1 (CH_{pyr}), 130.8 (NCMe), 128.1 (CH_{pyr}), 122.7 (CH_{pyr}), 118.1 (NCMe), 45.9 (N– CH_3), 4.7 (NCCH_3), 1.1 (NCCH_3). HR-MS: m/z calculated for $\text{C}_{23}\text{H}_{23}\text{O}_2\text{N}_7\text{F}_6\text{PRu} [\text{M}-\text{PF}_6-\text{MeCN}]^+ = 676.0590$; found: 676.0593. Elemental Analysis: anal. calculated for $\text{C}_{25}\text{H}_{26}\text{F}_{12}\text{N}_8\text{O}_2\text{P}_2\text{Ru}$: C: 34.85; H: 3.04; N: 13.01. Found: C: 34.86; H: 3.02; N: 12.71.

Complex 2a: This complex was synthesized according to the same procedure as described for complex **1** starting from **L2** (419 mg, 0.645 mmol), $[\text{RuCl}_2(\text{cym})]_2$ (201 mg, 0.335 mmol), and Na_2CO_3 (218 mg, 2.0 mmol) in MeCN (150 mL) and was obtained as a red crystalline powder (505 mg, 96%). ^1H NMR (300 MHz, $\text{DMSO}-d_6$) δ 9.07 (s, 2H, H_{PYA}), 8.55 (d, $^3J_{\text{HH}} = 5.9$ Hz, 2H, H_{PYA}), 8.32 (d, $^3J_{\text{HH}} = 9.0$ Hz, 2H, H_{PYA}), 8.10–8.20 (m, 3H, H_{pyr}), 8.01 (dd, $^3J_{\text{HH}} = 9.0, 5.9$ Hz, 2H, H_{PYA}), 4.37 (s, 6H, N– CH_3), 2.65 (s, 3H, NCCH_3), 2.34 (s, 6H, NCCH_3). ^{13}C NMR (101 MHz, $\text{DMSO}-d_6$) δ 169.4 (CO), 153.6 (C_{pyr}), 151.8 (C_{pyr}), 144.0 (CH_{pyr}), 143.0 (CH_{pyr}), 139.9 (CH_{pyr}), 139.5 (CH_{pyr}), 127.2 (CH_{pyr}), 125.3 (CH_{pyr}), 125.1 (NCMe), 118.1 (NCMe), 47.7 (N– CH_3), 3.8 (NCCH_3), 1.1 (NCCH_3). HR-MS: m/z calculated for $\text{C}_{25}\text{H}_{26}\text{F}_6\text{N}_8\text{O}_2\text{PRu} [\text{M}-\text{PF}_6]^+ = 717.0862$; found: 717.0859. Elemental Analysis: anal. calculated for $\text{C}_{25}\text{H}_{26}\text{F}_{12}\text{N}_8\text{O}_2\text{P}_2\text{Ru}$: C: 34.85, H: 3.04, N: 13.01. Found: C: 35.50, H: 3.63, N: 12.50.

General procedure for the synthesis of complexes 2b–f. Compound **2a** (1.0 eq.) and the indicated ligand were dissolved in EtOH (50 mL) and heated to reflux at 90 °C for 16 h. The mixture was cooled to rt and evaporated to dryness. The residue was dissolved in a minimum amount of MeCN and precipitated by addition of Et_2O . The precipitate was filtered, and washed with Et_2O , and dried in vacuo to yield the title complex as a crystalline powder.

Complex 2b: According to the general procedure from **2a** (97 mg, 0.113 mmol, 1.0 eq.) and 1,1-bis(diphenylphosphino)methane (92 mg, 0.120 mmol). Compound **2b** was obtained as orange crystalline powder (106 mg, 79%). ^1H NMR (400 MHz, $\text{MeCN}-d_3$) δ 8.35–8.39 (m, 1H, H_{pyr}), 8.27–8.29 (m, 2H, H_{pyr}), 7.75 (s, 1H, H_{PYA}), 7.73 (s, 1H, H_{PYA}), 7.44–7.46 (m, 2H, H_{PYA}), 7.43–7.37 (m, 4H, H_{Ph}), 7.30–7.34 (m, 2H, H_{PYA}), 7.27–7.18 (m, 8H, H_{Ph}), 7.16–7.05 (m, 8H, H_{Ph}), 6.94–6.98 (m, 2H, H_{PYA}), 4.72 (d, $^2J_{\text{HH}} = 10.1$ Hz, 1H, CH_2), 4.69 (d, $^2J_{\text{HH}} = 10.1$ Hz, 1H, CH_2), 3.85 (s, 6H, N– CH_3). ^{13}C NMR (101 MHz, $\text{MeCN}-d_3$) δ 170.3

(CO), 154.6 (C_{pyr}), 152.5 (C_{pyr}), 143.8 (CH_{pyr}), 143.2 (CH_{pyr}), 139.7 (CH_{pyr}), 139.2 (CH_{pyr}), 134.7 ($^1J_{\text{CP}} = 37$ Hz, $^3J_{\text{CP}} = 4.2$ Hz, C_{Ph}), 134.3 ($^1J_{\text{CP}} = 33$ Hz, $^3J_{\text{CP}} = 3.6$ Hz, C_{Ph}), 132.1 ($J_{\text{CP}} = 11.2$ Hz, CH_{Ph}), 131.8 ($J_{\text{CP}} = 2.6$ Hz, CH_{Ph}), 131.4 ($J_{\text{CP}} = 10.3$ Hz, CH_{Ph}), 131.2 ($J_{\text{CP}} = 2.4$ Hz, CH_{Ph}), 130.4 ($J_{\text{CP}} = 10.0$ Hz, CH_{Ph}), 129.9 ($J_{\text{CP}} = 9.7$ Hz, CH_{Ph}), 128.0 (CH_{pyr}), 127.1 (CH_{pyr}), 48.9 (N-CH₃), 43.0 (t, $^1J_{\text{CP}} = 26$ Hz, CH₂). $^{31}\text{P}\{^1\text{H}\}$ NMR (162 MHz, MeCN-*d*₃) δ 0.14 (d, $^2J_{\text{PP}} = 57.8$ Hz, 1P, dppm), -3.24 (d, $^2J_{\text{PP}} = 57.8$ Hz, 1P, dppm), -144.59 (hept, $^1J_{\text{PF}} = 708$ Hz, 2P, PF₆). HR-MS: m/z calculated for C₄₄H₃₉O₂N₅F₆P₃Ru [M-PF₆-MeCN]⁺ = 978.1259; found 978.1259. Elemental Analysis: anal. calculated for C₄₆H₄₂F₁₂N₆O₂P₄Ru × H₂O: C: 46.75, H: 3.75, N: 7.11. Found: C: 46.70, H: 4.13, N: 6.90.

Complex 2c: According to general procedures with compound **2a** (117 mg, 0.136 mmol, 1.0 eq.) and 1,2-bis(diphenylphosphino)ethane (56 mg, 0.141 mmol, 1.0 eq.). Compound **2c** was obtained as orange crystalline powder (137 mg, 0.116 mmol, 99% yield). ^1H NMR (300 MHz, DMSO-*d*₆) δ 8.50 (t, $^3J_{\text{HH}} = 7.8$ Hz, 1H, H_{pyr}), 8.26 (d, $^3J_{\text{HH}} = 7.8$ Hz, 2H, H_{pyr}), 8.06 (d, $^3J_{\text{HH}} = 6.9$ Hz, 2H, H_{PYA}), 7.66 (s, 2H, H_{PYA}), 7.31 (dd, $^3J_{\text{HH}} = 6.9, 8.4$ Hz, 2H, H_{PYA}), 7.28–7.16 (m, 14H, H_{Ph}), 7.06–7.02 (m, 6H, H_{Ph}), 6.81 (d, $^3J_{\text{HH}} = 8.4$ Hz, 2H, H_{PYA}), 3.98 (s, 6H, N-CH₃), 3.06 (br m, 2H, P-CH₂), 2.81 (br m, 2H, P-CH₂). ^{13}C NMR (101 MHz, DMSO-*d*₆) δ 170.5 (CO), 154.1 (C_{pyr}), 150.8 (C_{pyr}), 142.9 (CH_{pyr}), 140.5 (CH_{pyr}), 139.5 (CH_{pyr}), 138.2 (CH_{pyr}), 134.9 ($^1J_{\text{CP}} = 36$ Hz, C_{Ph}), 130.8 (CH_{pyr}), 130.2 ($J_{\text{CP}} = 8.1$ Hz, CH_{Ph}), 128.9 ($J_{\text{CP}} = 9.5$ Hz, CH_{Ph}), 128.2 ($J_{\text{CP}} = 8.9$ Hz, CH_{Ph}), 126.7 (CH_{pyr}), 114.5 (NCMe), 47.4 (N-CH₃), 24.0 (P-CH₂), 22.0 (P-CH₂), 1.1 (NCCH₃). ^{31}P NMR (162 MHz, DMSO-*d*₆) δ 66.23 (d, $^3J_{\text{PP}} = 13.8$ Hz, 1P, dppe), 54.25 (d, $^3J_{\text{PP}} = 13.8$ Hz, 1P, dppe), -144.17 (hept, $^1J_{\text{PF}} = 711$ Hz, 2P, PF₆). HR-MS: m/z calculated for C₄₅H₄₁O₂N₅F₆P₃Ru [M-PF₆-MeCN]⁺ = 992.1415; found: 992.1430. Elemental Analysis: anal. calculated for C₄₇H₄₄F₁₂N₆O₂P₄Ru × H₂O: C: 47.21, H: 3.88, N: 7.03. Found: C: 47.19, H: 4.29, N: 6.79.

Complex 2d: According to general procedures with compound **2a** (96 mg, 0.111 mmol, 1.0 eq.) and triphenylphosphine (31 mg, 0.118 mmol, 1.0 eq.). Compound **2d** was obtained as red crystalline powder (100 mg, 0.077 mmol, 66% yield). ^1H NMR (400 MHz, MeCN-*d*₃) δ 8.33 (s, 2H, H_{PYA}), 8.24 (d, $^3J_{\text{HH}} = 8.5$, 2H, H_{PYA}), 8.18 (d, $^3J_{\text{HH}} = 6.0$, 2H, H_{PYA}), 7.88 (dd, $^3J_{\text{HH}} = 8.5, 6.0$ Hz, 2H, H_{PYA}), 7.76 (t, $^3J_{\text{HH}} = 7.7$ Hz, 1H, H_{pyr}), 7.60 (d, $^3J_{\text{HH}} = 7.7$ Hz, 2H, H_{pyr}), 7.24–7.28 (m, 3H, H_{Ph}), 6.99–7.04 (m, 6H, H_{Ph}), 6.89–6.94 (m, 6H, H_{Ph}), 4.13 (s, 6H, N-CH₃), 2.67 (s, 3H, NCCH₃). ^{13}C NMR (101 MHz, MeCN-*d*₃) δ 170.3 (CO), 156.1 (C_{pyr}), 152.6 (C_{pyr}), 143.8 (CH_{pyr}), 142.2 (CH_{pyr}), 138.1 (CH_{pyr}), 136.9 (CH_{pyr}), 133.5 ($J_{\text{CP}} = 10.6$ Hz, CH_{Ph}), 132.5 ($^1J_{\text{CP}} = 45$ Hz, C_{Ph}), 130.7 ($J_{\text{CP}} = 2.3$ Hz, CH_{Ph}), 129.0 ($J_{\text{CP}} = 9.3$ Hz, CH_{Ph}), 128.1 (CH_{pyr}), 126.9 (CH_{pyr}), 49.0 (N-CH₃), 5.4 (NCCH₃). ^{31}P NMR (162 MHz, MeCN-*d*₃) δ 51.6 (s, 1P, PPh₃), -144.62 (hept, $^1J_{\text{PF}} = 707$ Hz, 2P, PF₆). HR-MS: m/z calculated for C₃₇H₃₂O₂N₅F₆P₂Ru [M-PF₆-2 MeCN]⁺ = 856.0973; found 856.0985. Elemental Analysis: anal. calculated for C₄₁H₃₈F₁₂N₇O₂P₃Ru: C: 45.48, H: 3.54, N: 9.06. Found: C: 44.67, H: 4.81, N: 9.01.

Complex 2e: According to general procedures with compound **2a** (105 mg, 0.122 mmol, 1.0 eq.) and ethylenediamine (10 μ l, 0.150 mmol, 1.3 eq.). Compound **2e** was obtained as a brown crystalline powder (90 mg, 0.107 mmol, 93% yield). ^1H NMR (300 MHz, DMSO- d_6) δ 8.55 (d, $^3J_{\text{HH}} = 6.0$ Hz, 2H, H_{PYA}), 8.48 (s, 2H, H_{PYA}), 8.27 (d, $^3J_{\text{HH}} = 8.4$ Hz, 2H, H_{PYA}), 7.91 (dd, $^3J_{\text{HH}} = 8.4, 6.0$ Hz, 2H, H_{PYA}), 7.87–7.90 (m, 2H, H_{pyr}), 7.79–7.84 (m, 1H, H_{pyr}), 4.50 (br s, 2H, NH₂), 4.32 (s, 6H, N–CH₃), 2.47 (s, 3H, NCCH₃), 2.06 (br m, 2H, CH₂), 1.89 (br m, 2H, CH₂). ^{13}C NMR (101 MHz, DMSO- d_6) δ 171.3 (CO), 156.2 (C_{pyr}), 151.3 (C_{pyr}), 142.4 (CH_{pyr}), 141.5 (CH_{pyr}), 138.3 (CH_{pyr}), 135.8 (CH_{pyr}), 127.8 (CH_{pyr}), 126.6 (CH_{pyr}), 48.6 (N–CH₃), 45.7 (CH₂), 44.0 (CH₂), 1.6 (NCCH₃). HR-MS: m/z calculated for C₂₃H₂₈O₂N₈F₆PRu [M–PF₆]⁺ = 695.1015; found: 695.1032. Elemental Analysis: anal. calculated for C₂₃H₂₆F₁₂N₈O₂P₂Ru: C: 32.98, H: 3.13, N: 13.38. Found: C: 33.48, H: 4.62, N: 13.23.

Complex 2f: According to general procedures with compound **2a** (100 mg, 0.116 mmol, 1.0 eq.) and 4-picoline (20 μ l, 0.232 mmol, 2.0 eq.). Compound **2f** was obtained as a black powder (95 mg, 0.098 mmol, 85% yield). ^1H NMR (300 MHz, DMSO- d_6) δ 9.08 (s, 2H, H_{PYA}), 8.56 (d, $^3J_{\text{HH}} = 5.7$ Hz, 2H, H_{PYA}), 8.02–8.08 (m, 3H, H_{pyr}), 7.91 (dd, $^3J_{\text{HH}} = 8.6, 5.7$ Hz, 2H, H_{PYA}), 7.78 (d, $^3J_{\text{HH}} = 8.6$ Hz, 2H, H_{PYA}), 7.69 (d, $^3J_{\text{HH}} = 6.6$ Hz, 4H, H_{4-pic}), 7.06 (d, $^3J_{\text{HH}} = 6.6$ Hz, 4H, H_{4-pic}), 4.33 (s, 6H, N–CH₃), 2.67 (s, 3H, NCCH₃), 2.26 (s, 6H, CH₃ 4-pic). ^{13}C NMR (101 MHz, DMSO- d_6) δ 169.8 (CO), 156.6 (C_{pyr}), 152.4 (CH_{4-pic}), 149.4 (C_{pyr}), 148.0 (C_{4-pic}), 141.6 (CH_{pyr}), 139.5 (CH_{pyr}), 137.7 (CH_{pyr}), 134.8 (CH_{pyr}), 129.9 (NCMe), 127.1 (CH_{pyr}), 126.5 (CH_{pyr}), 125.9 (CH_{4-pic}), 47.9 (N–CH₃), 20.2 (CH₃ 4-pic), 4.2 (NCCH₃). HR-MS: m/z calculated for C₃₃H₃₄O₂N₈F₆PRu [M–PF₆]⁺ = 821.1485; found: 821.1528. Elemental Analysis: anal. calculated for C₃₃H₃₄F₁₂N₈O₂P₂Ru: C: 41.04, H: 3.55, N: 11.60. Found: C: 40.68, H: 4.52, N: 11.27.

General procedure for catalytic transfer hydrogenation. In a 10 mL one-neck round bottom flask, a mixture of the complex (0.01 mmol), either anisole (54 mg, 0.5 mmol) or hexamethylbenzene (40 mg, 0.25 mmol) or hexadecane (226 mg, 1.0 mmol) as internal standard, and KOH (2 M solution in H₂O, 50 μ L, 0.1 mmol) in *i*PrOH (5 mL) was mixed. Then, substrate (1.0 mmol) was added and the reaction mixture heated to reflux in an oil bath (110 °C). Time zero was set when the mixture reached reflux conditions (ca. 30 sec). Aliquots (ca. 0.1 mL) were taken at set times and dissolved in CDCl₃ (for NMR analysis) or diluted in *i*PrOH (for GC analysis). Conversions and yields were determined relative to anisole, hexamethylbenzene, or hexadecane as internal standards.

Crystal structure determinations. Suitable single crystals of **L1**, **1**, **2a–d** and **2f** were mounted in air at ambient conditions and measured on an *Oxford Diffraction SuperNova* area-detector diffractometer⁶⁵ using mirror optics monochromated Mo *K* α radiation ($\lambda = 0.71073$ Å) and Al filtered.⁶⁶ Data reduction was performed using the *CrysAlisPro*⁶⁵ program. The intensities were corrected for Lorentz and polarization effects, and an absorption correction based on the multi-scan method using SCALE3 ABSPACK in *CrysAlisPro*⁶⁵ was applied. The structure was solved by direct methods using *SHELXT*⁶⁷, which revealed

the positions of all not disordered non-hydrogen atoms. The non-hydrogen atoms were refined anisotropically. All H-atoms were placed in geometrically calculated positions and refined using a riding model where each H-atom was assigned a fixed isotropic displacement parameter with a value equal to 1.2Ueq of its parent atom (1.5Ueq for the methyl groups). Refinement of the structure was carried out on F^2 using full-matrix least-squares procedures, which minimized the function $\sum w(F_o^2 - F_c^2)^2$. The weighting scheme was based on counting statistics and included a factor to downweight the intense reflections. All calculations were performed using the *SHELXL-2014/7*⁶⁸ program. Co-crystallized acetonitrile molecules in the asymmetric unit were found in the crystals of compound **1** (two), complex **2c** (three), and complex **2f** (one). The crystal of complex **2d** contained one co-crystallized diethylether molecule in the asymmetric unit. In compounds **1** and **2a–c** one methylpyridinium group is conformationally disordered about two orientations. The geometries of the two moieties of disordered methylpyridinium group were constrained to be similar in **2a**. Remaining electron density in solvent accessible voids originating from heavily disordered co-crystallized acetonitrile was accounted for with the SQUEEZE function of PLATON⁶⁹ in compounds **1** and **2b**. If present, disordered acetonitrile molecules, methylpyridinium groups and PF₆ anions were restrained to standard values. Their ADP's were restrained by the SHELXL SIMU and DELU instructions. The ADP's of the second PF₆ anion were restrained by the SHELXL RIGU instruction. Further crystallographic details are compiled in Tables S3–S9. Crystallographic data for all structures have been deposited with the Cambridge Crystallographic Data Centre (CCDC) as supplementary publication numbers 1851796 (**L1**), 1851797 (**1**), 1851801 (**2a**), 1851800 (**2b**), 1851802 (**2c**), 1851798 (**2d**), and 1851799 (**2f**).

Supporting Information Available: Listings of synthetic details, analytical data of the ligands and complexes, NMR data of ligand exchange reactions, time-conversion profiles for transfer hydrogenation and discussion on the reduction of α,β -unsaturated ketones, NMR spectra of all compounds, and crystallographic details.

Acknowledgements

We are grateful for generous financial support from the Swiss National Science Foundation (project 2000021_162868, and R'equip projects) as well as the European Research Council (CoG 615653). We thank the group of Chemical Crystallography of the University of Bern (PD Dr. P. Macchi) for the crystallographic analysis.

Literature

- (1) Peris, E.; Crabtree, R. H. Key Factors in Pincer Ligand Design. *Chem. Soc. Rev.* **2018**, *47*, 1959–1968.
- (2) *Pincer Compounds: Chemistry and Applications*; Morales-Morales, D., Ed.; Elsevier: Amsterdam, NL, 2018.
- (3) *The Privileged Pincer-Metal Platform: Coordination Chemistry & Applications*; van Koten, G., Gossage, R. A., Eds.; Springer: Berlin, Germany, 2016.
- (4) *Pincer and Pincer-Type Complexes: Applications in Organic Synthesis and Catalysis*; Szabó, K. J., Wendt, O. F., Eds.; Wiley-VCH: Weinheim, Germany, 2014.
- (5) *Organometallic Pincer Chemistry*; van Koten, G., Milstein, D., Eds.; Springer: Berlin, Germany, 2013.
- (6) Albrecht, M.; Lindner, M. M. Cleavage of Unreactive Bonds with Pincer Metal Complexes. *Dalton. Trans.* **2011**, *40*, 8733–8744.
- (7) Selander, N.; Szabó, K. J. Catalysis by Palladium Pincer Complexes. *Chem. Rev.* **2011**, *111*, 2048–2076.
- (8) Choi, J.; MacArthur, A. H. R.; Brookhart, M.; Goldman, A. S. Dehydrogenation and Related Reactions Catalyzed by Iridium Pincer Complexes. *Chem. Rev.* **2011**, *111*, 1761–1779.
- (9) Van Der Boom, M. E.; Milstein, D. Cyclometalated Phosphine-Based Pincer Complexes: Mechanistic Insight in Catalysis, Coordination, and Bond Activation. *Chem. Rev.* **2003**, *103*, 1759–1792.
- (10) Albrecht, M.; Van Koten, G. Platinum Group Organometallics Based on “Pincer” Complexes: Sensors, Switches, and Catalysts. *Angew. Chem. Int. Ed.* **2001**, *40*, 3750–3781.
- (11) Moulton, C. J.; Shaw, B. L. Transition Metal-Carbon Bonds. Part XLII. Complexes of Nickel, Palladium, Platinum, Rhodium and Iridium with the Tridentate Ligand 2,6-Bis[(Di-*t*-Butylphosphino)Methyl]Phenyl. *J. Chem. Soc., Dalton. Trans.* **1976**, *0*, 1020–1024.
- (12) van Koten, G.; Timmer, K.; Noltes, J. G.; Spek, A. L. A Novel Type of Pt-C Interaction and a Model for the Final Stage in Reductive Elimination Processes Involving C-C Coupling at Pt; Synthesis and Molecular Geometry of [1,N,N'- η -2,6-Bis{(Dimethylamino)Methyl}-Toluene]Iodoplatinum(II) Tetrafluoroborate. *J. Chem. Soc., Chem. Comm.* **1978**, *0*, 250–252.

- (13) van Koten, G.; Jastrzebski, J. T. B. H.; Noltes, J. G.; Spek, A. L.; Schoone, J. C. Triorganotin Cations Stabilized by Intramolecular SnN Coordination; Synthesis and Characterization of {C,N,N'-2,6-Bis[(Dimethylamino)Methyl]Phenyl}diorganotin Bromides. *J. Organomet. Chem.* **1978**, *148*, 233–245.
- (14) Abbenhuis, H. C. L.; Nantko, F.; Haarman, H. F.; Grove, D. M.; Horn, E.; Kooijman, H.; Spek, A. L.; van Koten, G. Effect of Intramolecular Coordination on Tantalum-Alkylidene-Centered Reactions: Synthesis and Structure of a Tantalum-Olefin Adduct and a Tantalum-Zinc-Alkylidene Complex. *Angew. Chem. Int. Ed.* **1991**, *30*, 996–998.
- (15) Abbenhuis, H. C. L.; Feiken, N.; Grove, D. M.; Jastrzebski, J. T. B. H.; Kooijman, H.; van der Sluis, P.; Smeets, W. J. J.; Spek, A. L.; van Koten, G. Use of an Aryldiamine Pincer Ligand in the Study of Tantalum Alkylidene-Centered Reactivity: Tantalum-Mediated Alkene Synthesis via Reductive Rearrangements and Wittig-Type Reactions. *J. Am. Chem. Soc.* **1992**, *114*, 9773–9781.
- (16) van Beek, J. A. M.; van Koten, G.; Smeets, W. J. J.; Spek, A. L. Model for the Initial Stage in the Oxidative Addition of I₂ to Organoplatinum(II) Compounds. X-ray Structure of Square-Pyramidal [Pt^{II}I{C₆H₃(CH₂NMe₂)_{2-o,o'}}(η¹-I₂)] Containing a Linear Pt-I-I Arrangement. *J. Am. Chem. Soc.* **1986**, *108*, 5010–5011.
- (17) Vigalok, A.; Milstein, D. Metal-Stabilized Quinone and Thioquinone Methides. *J. Am. Chem. Soc.* **1997**, *119*, 7873–7874.
- (18) Vigalok, A.; Shimon, L. J. W.; Milstein, D. Methylene Arenium Cations via Quinone Methides and Xylylenes Stabilized by Metal Complexation. *J. Am. Chem. Soc.* **1998**, *120*, 477–483.
- (19) Albrecht, M.; Gossage, R. A.; Spek, A. L.; van Koten, G. Metal-Mediated C-C Bond Making and Breaking: First Direct Evidence for a Reversible Migration of a Benzyl Group along a Metal-Carbon Bond. *J. Am. Chem. Soc.* **1999**, *121*, 11898–11899.
- (20) Terheijden, J.; van Koten, G.; Vinke, I. C.; Spek, A. L. 1,2-Methyl Shift between Pt and the Coordinated Aryl Group in the Reaction of Methyl Iodide with 2,6-Bis[(Dimethylamino)Methyl]Phenyl-N,N',C Complexes of Platinum(II). X-Ray Crystal Structure of the Arenonium-Platinum Compound [Pt(o-Tolyl)(MeC₆H₃(CH₂NMe₂)_{2-o,o'})]I. *J. Am. Chem. Soc.* **1985**, *107*, 2891–2898.
- (21) Vigalok, A.; Rybtchinski, B.; Shimon, L. J. W.; Ben-David, Y.; Milstein, D. Metal-Stabilized Methylene Arenium and σ-Arenium Compounds: Synthesis, Structure, Reactivity, Charge Distribution, and Interconversion. *Organometallics* **1999**, *18*, 895–905.

- (22) Gunanathan, C.; Milstein, D. Bond Activation and Catalysis by Ruthenium Pincer Complexes. *Chem. Rev.* **2014**, *114*, 12024–12087.
- (23) Poverenov, E.; Milstein, D. Noninnocent Behavior of PCP and PCN Pincer Ligands of Late Metal Complexes. *Top. Organomet. Chem.* **2013**, *40*, 21–48.
- (24) Zhang, J.; Leitus, G.; Ben-David, Y.; Milstein, D. Facile Conversion of Alcohols into Esters and Dihydrogen Catalyzed by New Ruthenium Complexes. *J. Am. Chem. Soc.* **2005**, *127*, 10840–10841.
- (25) Gunanathan, C.; Milstein, D. Metal-Ligand Cooperation by Aromatization-Deaeromatization: A New Paradigm in Bond Activation and “Green” Catalysis. *Acc. Chem. Res.* **2011**, *44*, 588–602.
- (26) Ben-Ari, E.; Leitus, G.; Shimon, L. J. W.; Milstein, D. Metal-Ligand Cooperation in C-H and H₂ Activation by an Electron-Rich PNP Ir(I) System: Facile Ligand Dearomatization-Aromatization as Key Steps. *J. Am. Chem. Soc.* **2006**, *128*, 15390–15391.
- (27) Khusnutdinova, J. R.; Milstein, D. Metal-Ligand Cooperation. *Angew. Chem. Int. Ed.* **2015**, *54*, 12236–12273.
- (28) Khusnutdinova, J. R.; Garg, J. A.; Milstein, D. Combining Low-Pressure CO₂ Capture and Hydrogenation to Form Methanol. *ACS Catal.* **2015**, *5*, 2416–2422.
- (29) Kohl, S. W.; Weiner, L.; Schwartsburd, L.; Konstantinovski, L.; Shimon, L. J. W.; Ben-David, Y.; Iron, M. A.; Milstein, D. Consecutive Thermal H₂ and Light-Induced O₂ Evolution from Water Promoted by a Metal Complex. *Science* **2009**, *324*, 74–77.
- (30) Gunanathan, C.; Ben-David, Y.; Milstein, D. Direct Synthesis of Amides from Alcohols and Amines with Liberation of H₂. *Science* **2007**, *317*, 790–792.
- (31) Shvo, Y.; Czarkie, D.; Rahamim, Y.; Chodosh, D. F. A New Group of Ruthenium Complexes: Structure and Catalysis. *J. Am. Chem. Soc.* **1986**, *108*, 7400–7402.
- (32) Noyori, R.; Ohkuma, T.; Kitamura, M.; Takaya, H.; Sayo, N.; Kumobayashi, H.; Akutagawa, S. Asymmetric Hydrogenation of β -Keto Carboxylic Esters. A Practical, Purely Chemical Access to β -Hydroxy Esters in High Enantiomeric Purity. *J. Am. Chem. Soc.* **1987**, *109*, 5856–5858.
- (33) Schneck, F.; Finger, M.; Tromp, M.; Schneider, S. Chemical Non-Innocence of an Aliphatic PNP Pincer Ligand. *Chem. Eur. J.* **2017**, *23*, 33–37.
- (34) Rösler, S.; Obenauf, J.; Kempe, R. A Highly Active and Easily Accessible Cobalt Catalyst for Selective Hydrogenation of C=O Bonds. *J. Am. Chem. Soc.* **2015**, *137*, 7998–8001.

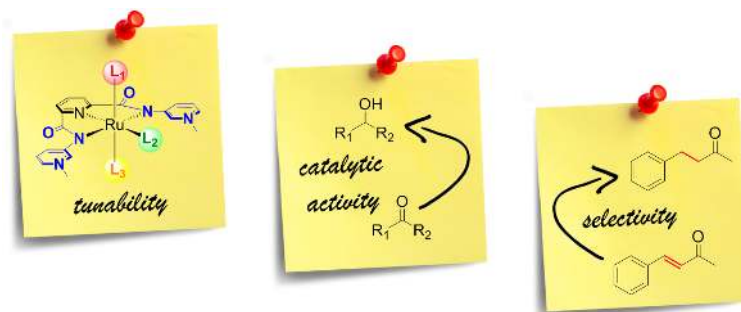
- (35) Thatcher, R. J.; Johnson, D. G.; Slattery, J. M.; Douthwaite, R. E. Charged Behaviour from Neutral Ligands: Synthesis and Properties of N-Heterocyclic Pseudo-Amides. *Chem. Eur. J.* **2012**, *18*, 4329–4336.
- (36) Shi, Q.; Thatcher, R. J.; Slattery, J.; Sauari, P. S.; Whitwood, A. C.; McGowan, P. C.; Douthwaite, R. E. Synthesis, Coordination Chemistry and Bonding of Strong N-Donor Ligands Incorporating the 1*H*-Pyridin-(2*E*)-Ylidene (PYE) Motif. *Chem. Eur. J.* **2009**, *15*, 11346–11360.
- (37) Brzezinski, B.; Zundel, G. An Intramolecular Charge Relay System via Easily Polarizable Hydrogen Bonds in the *N*-(4-Methyl-2-Pyridyl)Amide of 6-Methylpicolinic Acid *N*-Oxide. *J. Phys. Chem.* **1979**, *83*, 1787–1789.
- (38) Chien, C. H.; Leung, M. K.; Su, J. K.; Li, G. H.; Liu, Y. H.; Wang, Y. Substituent Effects on Pyridin-2-yl Ureas toward Intramolecular Hydrogen Bonding and Cytosine Complexation. *J. Org. Chem.* **2004**, *69*, 1866–1871.
- (39) Rais, D.; Gould, I. R.; Vilar, R.; White, A. J. P.; Williams, D. J. Structural and Theoretical Studies of New Ruthenium-Amidato Complexes with Phenanthroline Ligands Containing H-Bonding Groups. *Eur. J. Inorg. Chem.* **2004**, 1865–1872.
- (40) Doster, M. E.; Johnson, S. A. Selective C–F Bond Activation of Tetrafluorobenzenes by Nickel(0) with a Nitrogen Donor Analogous to N-Heterocyclic Carbenes. *Angew. Chem. Int. Ed.* **2009**, *48*, 2185–2187.
- (41) Boyd, P. D. W.; Wright, L. J.; Zafar, M. N. Extending the Range of Neutral N-Donor Ligands Available for Metal Catalysts: *N*-[1-Alkylpyridin-4(1*H*)-Ylidene]Amides in Palladium-Catalyzed Cross-Coupling Reactions. *Inorg. Chem.* **2011**, *50*, 10522–10524.
- (42) Doster, M. E.; Hatnean, J. A.; Jetic, T.; Modi, S.; Johnson, S. A. Catalytic C–H Bond Stannylation: A New Regioselective Pathway to C–Sn Bonds via C–H Bond Functionalization. *J. Am. Chem. Soc.* **2010**, *132*, 11923–11925.
- (43) Doster, M. E.; Johnson, S. A. Carbon-Hydrogen Bond Stannylation and Alkylation Catalyzed by Nitrogen-Donor-Supported Nickel Complexes: Intermediates with Ni–Sn Bonds and Catalytic Carbostannylation of Ethylene with Organostannanes. *Organometallics* **2013**, *32*, 4174–4184.
- (44) Leigh, V.; Carleton, D. J.; Olguin, J.; Mueller-Bunz, H.; Wright, L. J.; Albrecht, M. Solvent-Dependent Switch of Ligand Donor Ability and Catalytic Activity of Ruthenium(II) Complexes Containing Pyridinylidene Amide (PYA) N-Heterocyclic Carbene Hybrid Ligands. *Inorg. Chem.* **2014**, *53*, 8054–8060.

- (45) Navarro, M.; Li, M.; Müller-Bunz, H.; Bernhard, S.; Albrecht, M. Donor-Flexible Nitrogen Ligands for Efficient Iridium-Catalyzed Water Oxidation Catalysis. *Chem. Eur. J.* **2016**, *22*, 6740–6745.
- (46) Navarro, M.; Smith, C. A.; Albrecht, M. Enhanced Catalytic Activity of Iridium(III) Complexes by Facile Modification of C,N-Bidentate Chelating Pyridylideneamide Ligands. *Inorg. Chem.* **2017**, *56*, 11688–11701.
- (47) Navarro, M.; Smith, C. A.; Li, M.; Bernhard, S.; Albrecht, M. Optimization of Synthetically Versatile Pyridylidene Amide Ligands for Efficient Iridium-Catalyzed Water Oxidation. *Chem. Eur. J.* **2018**, *24*, 6386–6398.
- (48) Navarro, M.; Li, M.; Bernhard, S.; Albrecht, M. A Mesoionic Nitrogen-Donor Ligand: Structure, Iridium Coordination, and Catalytic Effects. *Dalton Trans.* **2017**, *47*, 659–662.
- (49) Mesoionic compounds are defined by IUPAC as “dipolar five- (possibly six-) membered heterocyclic compounds in which both the negative and the positive charge are delocalized, for which a totally covalent structure cannot be written, and which cannot be represented satisfactorily by any one polar structure. The formal positive charge is associated with the ring atoms, and the formal negative charge is associated with ring atoms or an exocyclic nitrogen or chalcogen atom.” IUPAC. Compendium of Chemical Terminology, 2nd edn. Gold Book Compiled by A. D. McNaught and A. Wilkinson, Blackwell Scientific Publications, Oxford, 1997. XML on-line corrected version: <http://goldbook.iupac.org> (2006) created by M. Nic, J. Jirat, and B. Kosata updates compiled by A. Jenkins. ISBN 0- 9678550-9-8.
- (50) Schuster, O.; Yang, L.; Raubenheimer, H. G.; Albrecht, M. Beyond Conventional N-Heterocyclic Carbenes: Abnormal, Remote, and Other Classes of NHC Ligands with Reduced Heteroatom Stabilization. *Chem. Rev.* **2009**, *109*, 3445–3478.
- (51) Crabtree, R. H. Abnormal, Mesoionic and Remote N-Heterocyclic Carbene Complexes. *Coord. Chem. Rev.* **2013**, *257*, 755–766.
- (52) Donnelly, K. F.; Petronilho, A.; Albrecht, M. Application of 1,2,3-Triazolylidenes as Versatile NHC-Type Ligands: Synthesis, Properties, and Application in Catalysis and Beyond. *Chem. Commun.* **2013**, *49*, 1145–1159.
- (53) Dorazco-González, A.; Höpfl, H.; Medrano, F.; Yatsimirsky, A. K. Recognition of Anions and Neutral Guests by Dicationic Pyridine-2,6-Dicarboxamide Receptors. *J. Org. Chem.* **2010**, *75*, 2259–2273.

- (54) Wang, D.; Astruc, D. The Golden Age of Transfer Hydrogenation. *Chem. Rev.* **2015**, *115*, 6621–6686.
- (55) Coe, B. J.; Glenwright, S. J. Trans-Effects in Octahedral Transition Metal Complexes. *Coord. Chem. Rev.* **2000**, *203*, 5–80.
- (56) Complexes **2a**, **2e**, and **2f** show a second reversible redox process at higher potentials which was assigned to a Ru^{III/IV} transition at 1.65 V for **2e**, and 1.84 V for **2f** (Fig. S6, S7). No additional redox process was observed for complexes **2b–d** up to 2.1 V.
- (57) Clapham, S. E.; Hadzovic, A.; Morris, R. H. Mechanisms of the H₂-Hydrogenation and Transfer Hydrogenation of Polar Bonds Catalyzed by Ruthenium Hydride Complexes. *Coord. Chem. Rev.* **2004**, *248*, 2201–2237.
- (58) Moore, C. M.; Szymczak, N. K. 6,6'-Dihydroxy Terpyridine: A Proton-Responsive Bifunctional Ligand and Its Application in Catalytic Transfer Hydrogenation of Ketones. *Chem. Commun.* **2013**, *49*, 400–402.
- (59) Horn, S.; Gandolfi, C.; Albrecht, M. Transfer Hydrogenation of Ketones and Activated Olefins Using Chelating NHC Ruthenium Complexes. *Eur. J. Inorg. Chem.* **2011**, 2863–2868.
- (60) Meyer, N.; Lough, A. J.; Morris, R. H. Iron(II) Complexes for the Efficient Catalytic Asymmetric Transfer Hydrogenation of Ketones. *Chem. Eur. J.* **2009**, *15*, 5605–5610.
- (61) Noyori, R.; Ohkuma, T. Asymmetric Catalysis by Architectural and Functional Molecular Engineering: Practical Chemo- and Stereoselective Hydrogenation of Ketones. *Angew. Chem. Int. Ed.* **2001**, *40*, 40–73.
- (62) Liu, T.; Zeng, Y.; Zhang, H.; Wei, T.; Wu, X.; Li, N. Facile Pd-Catalyzed Chemoselective Transfer Hydrogenation of Olefins Using Formic Acid in Water. *Tetrahedron Lett.* **2016**, *57*, 4845–4849.
- (63) Baan, Z.; Finta, Z.; Keglevich, G.; Hermeecz, I. Unexpected Chemoselectivity in the Rhodium-Catalyzed Transfer Hydrogenation of α,β -Unsaturated Ketones in Ionic Liquids. *Green Chem.* **2009**, *11*, 1937–1940.
- (64) Connelly, N. G.; Geiger, W. E. Chemical Redox Agents for Organometallic Chemistry. *Chem. Rev.* **1996**, *96*, 877–910.
- (65) CrysAlisPro, Version 1.; Oxford Diffraction Ltd., Ed.; Yarnton, Oxfordshire, U.K., 2010.

- (66) Macchi, P.; Bürgi, H.-B.; Chimpri, A. S.; Hauser, J.; Gál, Z. Low-Energy Contamination of Mo Microsource X-Ray Radiation: Analysis and Solution of the Problem. *J. Appl. Cryst.* **2011**, *44*, 763–771.
- (67) Sheldrick, G. M. SHELXT - Integrated Space-Group and Crystal-Structure Determination. *Acta Crystallogr. Sect. A* **2015**, *71*, 3–8.
- (68) Sheldrick, G. M. Crystal Structure Refinement with SHELXL. *Acta Crystallogr. Sect. C* **2015**, *71*, 3–8.
- (69) Spek, A. L. PLATON SQUEEZE: A Tool for the Calculation of the Disordered Solvent Contribution to the Calculated Structure Factors. *Acta Crystallogr. Sect. C* **2015**, *71*, 9–18.

Table of Contents entry:



Pincer ligands containing pyridylidene amide donor groups impart unique electronic properties to the ruthenium center, which can be modulated by the type of pincer ligand and the ancillary ligands. This approach produces transfer hydrogenation catalysts with rationally tunable catalytic activity, and with reactivity that can be tailored to convert also challenging substrates.